SKI Report 2003:08

Research

Research and Development Program in Reactor Diagnostics and Monitoring with Neutron Noise Methods

Stage 8. Final report

I. Pázsit
C. Demazière
V. Arzhanov

January 2003

ISSN 1104–1374
ISRN SKI-R-03/08-SE

SKI PERSPECTIVE

How this project has contributed to SKI's research goals

The overall goals for SKI research are:

- to give a basis for SKI 's supervision
- to maintain and develop the competence and research capacity within areas which are important to reactor safety
- to contribute directly to the Swedish safety work.

Above all, this project has contributed to the strategical research goal of competence and research capacity by building up competence within the Department of Reactor Physics at Chalmers University of Technology regarding reactor physics, reactor dynamics and noise diagnostics. The project has also contributed to the research goal of giving a basis for SKI's supervision by developing methods for identification and localization of perturbations in reactor cores.

The report comprises stage 8 of a long-term research and development program. The results have been published in international journals and have been included in both licentiate- and doctor's degrees.

Project information:

Project manager:	Ninos Garis, Department of Reactor Technology, SKI
Project number:	14.5-010892-01161
Previous reports:	SKI report 95:14 (1995), 96:50 (1996), 97:31 (1997), 98:25 (1998), 99:33 (1999), 00:28 (2000), 01:27 (2001).

SKI Report 2003:08

Research

Research and Development Program in Reactor Diagnostics and Monitoring with Neutron Noise Methods

Stage 8. Final report

I. Pázsit
C. Demazière
V. Arzhanov

Department of Reactor Physics
Chalmers University of Technology (CTH)
SE-412 96 Göteborg
SWEDEN

January 2003

Table of contents

Research and Development Program in Reactor Diagnostics and Monitoring with Neutron Noise Methods: Stage 8

Summary

This report gives an account of the work performed by the Department of Reactor Physics, Chalmers University of Technology, in the frame of a research contract with the Swedish Nuclear Power Inspectorate (SKI), contract No. 14.5-010892-01161. The present report is based on work performed by Christophe Demazière, and Vasiliy Arzhanov, with Imre Pázsit being the project leader.

This report constitutes Stage 8 of a long-term research and development program concerning the development of diagnostics and monitoring methods for nuclear reactors. The long-term goals are elaborated in more detail in e.g. the Final Reports of stage 1 and 2 (SKI Rapport 95:14 and 96:50, Refs. [1] and [2]). Results up to stage 7 were reported in [1] - [7]. A brief proposal for the continuation of this program in stage 9 is also given at the end of the report.

The program executed in Stage 8 consists of three parts and the work performed in each part is summarized below.

Development of the neutron noise simulator and its application to the localisation of a channel instability in Forsmark-1

In Stage 7, an anomaly localisation algorithm was presented and applied to the Forsmark-1 channel instability event (January 1997, fuel cycle 16). This investigation was carried out with a set of static data that were typical of a generic Boiling Water Reactor (BWR) model, since no data except the Local Power Range Monitors (LPRMs) time signals recorded during the instability event were made accessible to us at that time. In the present Stage, these static data were obtained from Vattenfall Fuel AB, who used the SIMULATE-3 code.

The first Section of this report is thus devoted to this anomaly localisation but this time with a relevant set of data, both regarding the static core conditions and regarding the LPRMs time signals. The noise source pointed out by the localisation algorithm was once again found to be very close to an unseated fuel assembly discovered during the fuel outage following the instability event. The localisation procedure relies in fact on the prior calculation of the reactor transfer function, carried out via the neutron noise simulator first presented in Stage 6 and later improved in Stage 7.

The neutron noise simulator was also improved in this Stage. More precisely, a 2-D 2-group static core simulator was developed in order to calculate the static flux and the associated eigenvalue with a spatial discretisation scheme compatible with the one in use in the neutron noise simulator, i.e. finite differences.

A phenomenological model for the explanation of a strongly space-dependent Decay Ratio

It has generally been assumed that the Decay Ratio (DR), a parameter characterizing the stability of Boiling Water Reactors (BWRs), is a space-independent parameter of the reactor, i.e. it is independent of which Local Power Range Monitor (LPRM) is used in the core to perform its evaluation. However, a seemingly strongly space-dependent DR was found

during the Forsmark local instability event. The second Section of this report shows that the presence of two or more simultaneous types or sources of instability with different stability properties and with different space dependence renders the DR space-dependent, in some cases strongly space-dependent. Two cases were investigated: the case of a local noise source coexisting with a global noise source (in-phase oscillations) and the case of two local noise sources. The results of these calculations were compared to the Forsmark-1 channel instability event, which revealed that the DR was not homogeneous throughout the core. Good adequacy was found between the DR model applied to the Forsmark-1 event and the corresponding measured DR. The fact that one single noise source in the core does not allow explaining a non-homogeneous DR suggests that in the case of Forsmark-1, at least two types or sources of instability had to be present in the core at the same time. This is consistent with the experience found in the application of the localisation algorithm presented in the first Section of this report, since there it was shown that very likely at least two local noise sources were present in the core. According to the results obtained in this section, however, the two types of oscillations that explain the strongly space-dependent DR could be either a local and a global instability, or two local ones.

Continued analysis of the detector impacting with wavelets

Detection of impacting of detector tubes, also called instrument strings, have been a matter of interest both in Swedish and foreign BWRs. Although the detection of vibrations is relatively simple, the discovery and quantifying of the severity of impacting is far more complicated. There exists no single method that gives absolute results without the need for calibration or comparison with reference measurements.

The previous report presented a thorough investigation of all measurements made with the Haar wavelet function, which gave a reasonably good correlation of the impacting indicator with the reported damage, namely 0.38. As a comparison, the best non-wavelet based indicator, pp2 [7], showed a correlation of 0.43. This report extends the investigation to a broader set of wavelet functions. Wavelets available in MATLAB have now been tried. A general wavelet-based algorithm to evaluate the impacting rate has been developed. It uses only one model parameter, the fuel box eigenfrequency, that must be set a priori. The rest is done fully automatically. Given a wavelet function, the algorithm selects:

- the level of wavelet decomposition;
- the white noise component;
- the threshold to identify separate impactings.

As a result of the investigation, a sorted list of wavelets is presented where the best wavelet function shows a correlation of 0.53, which considerably improves the performance of the Haar wavelet and exceeds the best non-wavelet indicator reported in the previous report.

For the next stage we propose an investigation aimed at improving the algorithm performance in the following:

- more accurate estimate of the white noise component;
- more accurate estimate of the threshold.

Another possible direction of investigation could be to consider some of wavelets not included in MATLAB.

Forskningsprogram angående härddiagnostik och härdövervakning med neutronbrusmetoder: Etapp 8

Sammanfattning

Denna rapport redovisar det arbete som utförts inom ramen för ett forskningskontrakt mellan Avdelningen för Reaktorfysik, Chalmers tekniska högskola och Statens Kärnkraftinspektion (SKI), kontrakt Nr. 14.5-010892-01161. Rapporten är baserad på arbetsinsatser av Christophe Demazière och Vasiliy Arzhanov, med Imre Pázsit som projektledare.

Rapporten omfattar etapp 8 i ett långsiktigt forsknings- och utvecklingsprogram angående utveckling av diagnostik och övervakningsmetoder för kärnkraftreaktorer. De långsiktiga målen med programmet har utarbetats i slutrapporterna för etapp 1 och 2 (SKI Rapport 95:14 och 96:50, Ref. [1] och [2]). Uppnådda resultat fram till etapp 7 har redovisats i referenserna [1] - [7]. Ett förslag till fortsättning av programmet i etapp 9 redovisas i slutet av rapporten.

Det utförda forskningsarbetet i etapp 8 består av tre olika delar och arbetet i varje del sammanfattas nedan.

Vidareutveckling av neutronbrussimulatorn och dess tillämpning för lokalisering av kanalinstabiliteten i Forsmark-1

I etapp 7 presenterade vi en algoritm för lokalisering av anomalier och tillämpade den för lokalisering av kanalinstabiliteten i Forsmark-1 (januari 1997, bränslecykel 16). Tillämpningen i etapp 7 skedde genom användning av härddata, härrörande från en generisk kokvattenreaktormodell (BWR), eftersom vi då inte hade tillgång till Forsmarks härddata. I föreliggande etapp har vi erhållit dessa data från Vattenfall Bränsle AB, som använder koden SIMULATE-3. Genom detta erhöll vi data i en för oss användbar form.

Första kapitlet i denna rapport handlar således om lokalisering av kanalinstabiliteten med tillämping av de aktuella härddata som gällde vid mätningen, samt de upmätta LPRM tidssignalerna. Även inom denna studie har vi lokaliserat bruskällan i en härdposition som ligger ganska nära den osätade bränslepatron, som upptäcktes under revisionen efter instabilitetshändelsen.

Lokaliseringsproceduren använder de numeriska värdena av den dynamiska överföringsfunktionen, som beräknas genom den så kallade brussimulatorn, som vi beskrev först i etapp 6 och sedan vidareutvecklade i etapp 7. Brussimulatorn har emellertid förbättrats ytterligare i denna etapp. Mer konkret, en 2-D 2-group statisk härdsimulator har utvecklats för beräkning av den statiska flödestätheten och den tillhörande multiplikationsfaktorn (egenvärdet) med ett rumsdiskretisationsschema som är kompatibelt med brussimulatorns, nämligen finitdifferensmetoden.

En fenomenologisk modell för förklaringen av en stark rumsberoende dämpkvot (DR)

Den generella uppfattningen har varit att dämpkvoten (DR), det vill säga parametern som karakteriserar härdstabiliteten hos en kokvattenreaktor (BWR), är rumsoberoende, det vill säga dess värde beror inte på vilken LPRM-signal som används för dess bestämning. Under kanalinstabiliteten i Forsmark var DR emellertid till synes starkt rumsberoende. Andra kapitlet i denna rapport visar därför att samtidig närvaro av två eller flera slag av

bruskällor respektive instabiliteter, som har olika DR samt olika rumsberoende, gör DRn, som beräknas från enstaka LPRM, även rumsberoende, till och med starkt rumsberoende.

Vi har undersökt två huvudscenarier: ett fall när en lokal bruskälla och en global (in-phase) instabilitet verkar samtidigt, och ett fall när två lokala bruskällor verkar samtidigt. Resultaten från dessa fall jämfördes med mätningar från Forsmark-1-instabiliteten, där DR var starkt rumsberoende. Vi har funnit bra överensstämmelse mellan resultaten från den empiriska modellen för båda fallen, och från mätningen. Detta indikerar att under Forsmark-1-instabiliteten har minst två bruskällor eller instabiliteter varit verksamma. Detta stämmer överens med undersökningarna i Kapitel 2, där starka indikationer fanns om minst två lokala instabiliteter när det gäller Forsmark-mätningarna. Resultaten i föreliggande kapitel visar emellertid att en starkt rumsberoende dämpkvot kan förklaras såväl med en lokal och en global instabilitet, som med två lokala instabiliteter.

Fortsatt analys av detektorstötar med wavelet-teknik

Detektering av stötar av detektorsonder i BWR har varit föremål för undersökningar både i Sverige och utomlands. Medan upptäckten av vibrationer är enkel, är upptäckten och kvantifieringen av stötar och dess farlighetsgrad långt mer komplicerad. Det finns ingen enkel metod som ger slutsatser i absoluta termer utan behov av kalibrering eller jämförelse med referensmätningar.

I föregående rapport presenterade vi en omfattande undersökning med användning av Haar wavelet-funktionen. Den har givit en jämförelsevis bra korrelation av impakt-indikatorn med de experimentellt observerade skadorna på sonderna, nämligen 0.38. För jämförelse, har den bästa, icke-wavelet baserade metoden gett en korrelation av 0.43. I denna rapport har vi utvidgat undersökningen till ett bredare urval av wavelet- funktioner. Alla wavelet-funktioner som är tillgängliga i MATLAB har testats. En generisk wavelet-baserad algoritm har utvecklats för utvärdering av stötfrekvensen. Den använder sig av en enda modell-parameter som behöver anges i förväg, nämligen egen-frekvensen av bränsleboxarnas vibrationer vid stötar. Resten innehåller enbart standardiserade algoritmer. För en given utvald wavelet-funktion väljer algoritmen

- nivån av wavelet dekomposition;
- vitbrus-komponenten;
- tröskeln för identifiering av individuella stötar.

Undersökingens resultat har sammanfattats i en sorterad lista av wavelets, där den bästa funktionen visar en korrelation (“success rate”) av 0.53, vilket är avsevärt bättre än Haar wavelets prestanda, och även överskrider den bästa icke-wavelet baserade metoden som har redovisats i föregående rapporter.

För fortsättningen föreslår vi en undersöking med målet att förbättra prestandan ytterligare enligt följande:

- en noggrannare uppskattning av vitbrus-komponenten;
- en noggrannare uppskattning av tröskelvärdet.

En ytterligare möjlighet är att undersöka wavelet-funktioner som är ej inkluderade i MATLAB.

Section 1

Development of the neutron noise simulator and its application to the localisation of a channel instability in Forsmark-1

1.1 Introduction

In Stage 7, a localisation algorithm was developed [7]. This localisation algorithm is able to give the location of a noise source (if it exists) of any core if one has access to the noise signals delivered by a few (at least three) Local Power Range Monitors (LPRMs) located on the same axial plane. This localisation procedure relies on the neutron noise simulator first developed in Stage 6 [6], and later improved in Stage 7 [7].

The localisation algorithm was used in a real case, namely the Forsmark-1 channel instability event (January 1997, fuel cycle 16), since a stability measurement was carried out at that occasion. During this measurement, the lower plane of the core was rather well equipped with LPRMs (27 of the 36 available detector strings were actually recorded). Nevertheless, it was not possible for this first application of the localisation algorithm to get any realistic data regarding the core itself, data that are necessary in order to use the neutron noise simulator (material constants, point-kinetic parameters of the core, and static fluxes). In this Stage, such data were obtained from Vattenfall Fuel AB, via the SIMULATE-3 code [8]. The localisation algorithm was thus applied again to the Forsmark-1 case, but this time with realistic data. The preparation of the data to be used in the localisation algorithm is presented in Section 1.2, whereas the results of the new localisation search are presented in Section 1.4.

Another improvement compared to Stage 7 is the development of a 2-D 2-group static core simulator, compatible with and coupled to the neutron noise simulator. It was pointed out in Stage 7 that the static flux and the corresponding eigenvalue had to be calculated with a spatial discretisation scheme compatible with the one used in the neutron noise simulator, otherwise this would be equivalent to make the system non-critical. Nevertheless, recalculating the static flux and the corresponding eigenvalue with a finite difference scheme, scheme used in the neutron noise simulator, is identical to neglect the main advantage of using a commercial core simulator like SIMULATE-3, i.e. its accuracy. This is why another approach was preferred in Stage 7. This approach was simpler since no calculation of the static flux and eigenvalue was required. The static flux of the SIMULATE-3 core simulator was in fact directly used to adjust the static cross-sections so that the balance equations were fulfilled in each node with the finite difference scheme. This was completely equivalent to make the system critical with the most accurate set of fluxes available and with a scheme compatible with the one used in the noise estimation.

The balance equations that needed to be fulfilled were given as:

$$[D_1(\boldsymbol{r})\Delta\phi_1(\boldsymbol{r})]_{(I,J)} + \frac{\nu\Sigma_{f,1,I,J}}{k_{eff}}\phi_{1,I,J} + \frac{\nu\Sigma_{f,2(1),I,J}}{k_{eff}}\phi_{2,I,J} - \Sigma_{a,1,I,J}\phi_{1,I,J} - \Sigma_{rem,I,J}\phi_{1,I,J} = 0 \quad (1)$$

$$[D_2(\boldsymbol{r})\Delta\phi_2(\boldsymbol{r})]_{(I,J)} + \Sigma_{rem,I,J}\phi_{1,I,J} - \Sigma_{a,2,I,J}\phi_{2,I,J} = 0 \quad (2)$$

with the leakage terms estimated according to the finite difference scheme below:

$$[D_1(\boldsymbol{r})\Delta\phi_1(\boldsymbol{r})]_{(I,J)} = \left(\frac{a^x_{1,I,J}}{\Delta x}+\frac{a^y_{1,I,J}}{\Delta y}\right)\phi_{1,I,J} + \frac{b^x_{1,I,J}}{\Delta x}\phi_{1,I+1,J} + \frac{b^y_{1,I,J}}{\Delta y}\phi_{1,I,J+1} + \frac{c^x_{1,I,J}}{\Delta x}\phi_{1,I-1,J} + \frac{c^y_{1,I,J}}{\Delta y}\phi_{1,I,J-1} \quad (3)$$

$$[D_2(\boldsymbol{r})\Delta\phi_2(\boldsymbol{r})]_{(I,J)} = \left(\frac{a^x_{2,I,J}}{\Delta x}+\frac{a^y_{2,I,J}}{\Delta y}\right)\phi_{2,I,J} + \frac{b^x_{2,I,J}}{\Delta x}\phi_{2,I+1,J} + \frac{b^y_{2,I,J}}{\Delta y}\phi_{2,I,J+1} + \frac{c^x_{2,I,J}}{\Delta x}\phi_{2,I-1,J} + \frac{c^y_{2,I,J}}{\Delta y}\phi_{2,I,J-1} \quad (4)$$

The different coefficients $a^x_{G,I,J}$, $a^y_{G,I,J}$, $b^x_{G,I,J}$, $b^y_{G,I,J}$, $c^x_{G,I,J}$, and $c^y_{G,I,J}$ are summarised in Table I and Table II for the *x* and *y* directions, respectively.

Table I. Coupling coefficients in the *x* direction.

	$a^x_{G,I,J}$	$b^x_{G,I,J}$	$c^x_{G,I,J}$
if the node *I-1* does not exist	$\frac{2D_{G,I,J}D_{G,I+1,J}}{\Delta x(D_{G,I,J}+D_{G,I+1,J})} + \frac{2D_{G,I,J}}{\Delta x}$	$-\frac{2D_{G,I,J}D_{G,I+1,J}}{\Delta x(D_{G,I,J}+D_{G,I+1,J})}$	0
if the nodes *I-1* and *I+1* both exist	$\frac{2D_{G,I,J}D_{G,I+1,J}}{\Delta x(D_{G,I,J}+D_{G,I+1,J})} + \frac{2D_{G,I,J}D_{G,I-1,J}}{\Delta x(D_{G,I,J}+D_{G,I-1,J})}$	$-\frac{2D_{G,I,J}D_{G,I+1,J}}{\Delta x(D_{G,I,J}+D_{G,I+1,J})}$	$-\frac{2D_{G,I,J}D_{G,I-1,J}}{\Delta x(D_{G,I,J}+D_{G,I-1,J})}$
if the node *I+1* does not exist	$\frac{2D_{G,I,J}}{\Delta x} + \frac{2D_{G,I,J}D_{G,I-1,J}}{\Delta x(D_{G,I,J}+D_{G,I-1,J})}$	0	$-\frac{2D_{G,I,J}D_{G,I-1,J}}{\Delta x(D_{G,I,J}+D_{G,I-1,J})}$

Table II. Coupling coefficients in the *y* direction.

	$a^y_{G,I,J}$	$b^y_{G,I,J}$	$c^y_{G,I,J}$
if the node *J-1* does not exist	$\frac{2D_{G,I,J}D_{G,I,J+1}}{\Delta y(D_{G,I,J}+D_{G,I,J+1})} + \frac{2D_{G,I,J}}{\Delta y}$	$-\frac{2D_{G,I,J}D_{G,I,J+1}}{\Delta y(D_{G,I,J}+D_{G,I,J+1})}$	0

Table II. Coupling coefficients in the *y* direction.

	$a^{y}_{G,I,J}$	$b^{y}_{G,I,J}$	$c^{y}_{G,I,J}$
if the nodes *J-1* and *J+1* both exist	$\frac{2D_{G,I,J}D_{G,I,J+1}}{\Delta y(D_{G,I,J}+D_{G,I,J+1})} + \frac{2D_{G,I,J}D_{G,I,J-1}}{\Delta y(D_{G,I,J}+D_{G,I,J-1})}$	$-\frac{2D_{G,I,J}D_{G,I,J+1}}{\Delta y(D_{G,I,J}+D_{G,I,J+1})}$	$-\frac{2D_{G,I,J}D_{G,I,J-1}}{\Delta y(D_{G,I,J}+D_{G,I,J-1})}$
if the node *J+1* does not exist	$\frac{2D_{G,I,J}}{\Delta y} + \frac{2D_{G,I,J}D_{G,I,J-1}}{\Delta y(D_{G,I,J}+D_{G,I,J-1})}$	0	$-\frac{2D_{G,I,J}D_{G,I,J-1}}{\Delta y(D_{G,I,J}+D_{G,I,J-1})}$

The following procedure was then applied for the adjustment of the cross-sections. First, the thermal absorption cross-section was modified to fulfil Eqs. (2) and (4). If such an adjustment was not possible (because it would result in a negative cross-section), the removal cross-section was modified instead, and the eigenvalue modified so that Eqs. (1) and (3) could be fulfilled. If this too was impossible, the fast absorption cross-section could also be modified. For the reflector nodes, an adjustment of the absorption cross-sections (both fast and thermal) was first carried out. In case of negative results, the removal cross-section was modified. But due to the coupling between the fast and thermal groups and the relatively few number of parameters that can be changed, an iterative procedure was required if the removal cross-section was adjusted in the reflector nodes. As a matter of fact, this procedure only affects appreciably the cross-sections in the reflector nodes, and to a lesser extent the cross-sections of the fuel nodes immediately neighbouring the reflector. The main reason lies with the fact that a finite difference scheme does not estimate the static flux accurately in these nodes when only a few nodes are used for the calculation. When this procedure was applied to the realistic data corresponding to Forsmark-1, negative removal cross-sections were obtained in the reflector nodes and the iteration process, which was supposed to correct for this effect, did not converge. Consequently, when using strongly heterogeneous data like for instance in BWR cases, it is required to recalculate the static flux and the eigenvalue according to a finite difference scheme, i.e. a spatial discretisation scheme compatible with the one in use in the neutron noise simulator. Such a static core simulator is presented in the following Section 1.3.

1.2 Preparation of the Forsmark-1 data for the localisation procedure

As will be seen in the following, the 2-D 2-group material data and the point-kinetic parameters of the core are required for the localisation algorithm, and thus for the calculation of the induced neutron noise via the noise simulator. Furthermore, the static flux is also needed for the static core simulator as an initial guess in the iteration process (see Section 1.3).

Hence, the 2-group cross-sections provided by SIMULATE-3 for each node were homogenised from 3-D to 2-D in order to be used by the 2-D simulators. The homogenization was naturally carried out by using the static fluxes as weighting functions so that the reaction rates were preserved:

$$XS_{G,I,J} = \frac{\sum_K XS_{G,I,J,K}\phi_{G,I,J,K}V_{I,J,K}}{\sum_K \phi_{G,I,J,K}V_{I,J,K}} \tag{5}$$

and

$$\phi_{G,I,J} = \frac{\sum_K \phi_{G,I,J,K}V_{I,J,K}}{\sum_K V_{I,J,K}} \tag{6}$$

with XS_G having a broad meaning, i.e. being D_G, $\Sigma_{a,G}$, Σ_{rem}, or $\nu\Sigma_{f,G}$. All the other symbols have their usual meaning with $V_{I,J,K}$ representing the volume of the node *(I,J,K)*. G is the group index ($G = 1$ for the fast group, and $G = 2$ for the thermal group).

Although this way of averaging the material data and the fluxes preserves the reaction rates, the 2-D system which is thus obtained will have a much higher eigenvalue than the 3-D system since the leakage in the axial direction was eliminated (a 2-D system is in fact assumed to be infinite in the third direction). Therefore, if one wants results compatible with the actual 3-D core, one has to take the axial leakage into account in the 2-D system. This can be done by increasing the absorption cross-section in each group by an artificial leakage cross-section in the same group, which allows having the correct leakage rate when multiplied by the corresponding group flux. For that purpose, one needs to evaluate the axial leakage rate in each node for the 3-D system. Since this leakage rate is not given by SIMULATE-3, the finite difference scheme is used instead (this finite difference scheme is also used in the static core simulator, and the neutron noise simulator). In the "box-scheme" approximation, this reads as [9]:

$$\begin{aligned} &\text{leakage rate in group } G \text{ and node}(I,J,K) \\ &= -\frac{1}{\Delta z}[a^z_{G,I,J,K}\phi_{G,I,J,K} + b^z_{G,I,J,K}\phi_{G,I,J,K+1} + c^z_{G,I,J,K}\phi_{G,I,J,K-1}] \\ &= LR_{G,I,J,K} \end{aligned} \tag{7}$$

with the coefficients $a^z_{G,I,J,K}$, $b^z_{G,I,J,K}$, and $c^z_{G,I,J,K}$ given by the following Table III.

Table III. Coupling coefficients in the z direction.

	$a^z_{G,I,J,K}$	$b^z_{G,I,J,K}$	$c^z_{G,I,J,K}$
if the node *K-1* does not exist	$\frac{2D_{G,I,J,K}D_{G,I,J,K+1}}{\Delta z(D_{G,I,J,K}+D_{G,I,J,K+1})} + \frac{2D_{G,I,J,K}}{\Delta z}$	$-\frac{2D_{G,I,J,K}D_{G,I,J,K+1}}{\Delta z(D_{G,I,J,K}+D_{G,I,J,K+1})}$	0

Table III. Coupling coefficients in the *z* direction.

	$a^z_{G,I,J,K}$	$b^z_{G,I,J,K}$	$c^z_{G,I,J,K}$
if the nodes *K-1* and *K+1* both exist	$\frac{2D_{G,I,J,K}D_{G,I,J,K+1}}{\Delta z(D_{G,I,J,K}+D_{G,I,J,K+1})} + \frac{2D_{G,I,J}D_{G,I,J,K-1}}{\Delta z(D_{G,I,J,K}+D_{G,I,J,K-1})}$	$-\frac{2D_{G,I,J,K}D_{G,I,J,K+1}}{\Delta z(D_{G,I,J,K}+D_{G,I,J,K+1})}$	$-\frac{2D_{G,I,J,K}D_{G,I,J,K-1}}{\Delta z(D_{G,I,J,K}+D_{G,I,J,K-1})}$
if the node *K+1* does not exist	$\frac{2D_{G,I,J,K}}{\Delta z} + \frac{2D_{G,I,J,K}D_{G,I,J,K-1}}{\Delta z(D_{G,I,J,K}+D_{G,I,J,K-1})}$	0	$-\frac{2D_{G,I,J,K}D_{G,I,J,K-1}}{\Delta z(D_{G,I,J,K}+D_{G,I,J,K-1})}$

The corresponding “leakage” cross-sections are thus given by:

$$L_{G,I,J,K} = -\frac{LR_{G,I,J,K}}{\phi_{G,I,J,K}} \tag{8}$$

so that the absorption cross-sections are modified in the following way:

$$\Sigma^*_{a,G,I,J,K} = \Sigma_{a,G,I,J,K} + L_{G,I,J,K} \tag{9}$$

Then the homogenization is carried out as described before, i.e. according to Eq. (5).

1.3 Development of a static core simulator coupled to the neutron noise simulator

As was explained previously, the neutron noise simulator requires not only the 2-D 2-group material constants and the point-kinetic parameters of the core, but also the 2-D 2-group static fluxes and the corresponding eigenvalue. Consequently, the neutron noise simulator has to be used with a static core simulator that is compatible with the neutron noise simulator, i.e. that has the same spatial discretisation scheme. In the following, the main characteristics of this static core simulator and a benchmark for BWR cores are presented.

In the two-group diffusion approximation, the static flux is the solution of the following matrix equation:

$$[\bar{\bar{D}}(\boldsymbol{r})\nabla^2 + \bar{\bar{\Sigma}}(\boldsymbol{r})] \times \begin{bmatrix} \phi_1(\boldsymbol{r}) \\ \phi_2(\boldsymbol{r}) \end{bmatrix} = 0 \tag{10}$$

where

$$\overline{\overline{D}}(\boldsymbol{r}) = \begin{bmatrix} D_1(\boldsymbol{r}) & 0 \\ 0 & D_2(\boldsymbol{r}) \end{bmatrix} \tag{11}$$

$$\overline{\overline{\Sigma}}(\boldsymbol{r}) = \begin{bmatrix} \frac{\nu\Sigma_{f,1}(\boldsymbol{r})}{k_{eff}} - \Sigma_{a,1}(\boldsymbol{r}) - \Sigma_{rem}(\boldsymbol{r}) & \frac{\nu\Sigma_{f,2}(\boldsymbol{r})}{k_{eff}} \\ \Sigma_{rem}(\boldsymbol{r}) & -\Sigma_{a,2}(\boldsymbol{r}) \end{bmatrix} \tag{12}$$

This system of equations has to be spatially discretised. Finite differences were used for that task, and more precisely the so-called "box-scheme" (more information regarding this specific point can be found in [6] and [7], where the discretisation scheme was extensively explained):

$$\begin{aligned} &\frac{1}{\Delta x \cdot \Delta y} \int_{(I,J)} D_G(\boldsymbol{r}) \nabla^2 \phi_G(\boldsymbol{r}) d\boldsymbol{r} \\ &= -\frac{(a^x_{G,I,J}\phi_{G,I,J} + b^x_{G,I,J}\phi_{G,I+1,J} + c^x_{G,I,J}\phi_{G,I-1,J})}{\Delta x} \\ &-\frac{(a^y_{G,I,J}\phi_{G,I,J} + b^y_{G,I,J}\phi_{G,I,J+1} + c^y_{G,I,J}\phi_{G,I,J-1})}{\Delta y} \end{aligned} \tag{13}$$

with the different coefficients $a^x_{G,I,J}$, $a^y_{G,I,J}$, $b^x_{G,I,J}$, $b^y_{G,I,J}$, $c^x_{G,I,J}$, and $c^y_{G,I,J}$ summarised in Table I and Table II for the x and y directions respectively.

The matrix equation given by Eq. (10) has to be used to determine both the two-group fluxes and the eigenvalue. This can be done via the so-called outer iteration that can be summarised as follows. If one rewrites Eqs. (10) - (12) as:

$$\overline{\overline{M}}(\boldsymbol{r}) \times \bar{\phi}(\boldsymbol{r}) = \frac{1}{k_{eff}} \overline{\overline{F}}(\boldsymbol{r}) \times \bar{\phi}(\boldsymbol{r}) \tag{14}$$

with

$$\overline{\overline{M}}(\boldsymbol{r}) = \begin{bmatrix} \Sigma_{a,1}(\boldsymbol{r}) + \Sigma_{rem}(\boldsymbol{r}) - D_1(\boldsymbol{r})\nabla^2 & 0 \\ -\Sigma_{rem}(\boldsymbol{r}) & \Sigma_{a,2}(\boldsymbol{r}) - D_2(\boldsymbol{r})\nabla^2 \end{bmatrix} \tag{15}$$

$$\overline{\overline{F}}(\boldsymbol{r}) = \begin{bmatrix} \nu\Sigma_{f,1}(\boldsymbol{r}) & \nu\Sigma_{f,2}(\boldsymbol{r}) \\ 0 & 0 \end{bmatrix} \tag{16}$$

$$\bar{\phi}(\boldsymbol{r}) = \begin{bmatrix} \phi_1(\boldsymbol{r}) \\ \phi_2(\boldsymbol{r}) \end{bmatrix} \tag{17}$$

then the flux and the eigenvalue can be searched for by using an iterative scheme. In the present study, the power iteration method was chosen for its simplicity and its relative efficiency [9], [10]. In such a method, the flux and the eigenvalue are given by the following expressions:

$$\bar{\phi}^{(n)}(\boldsymbol{r}) = \overline{\overline{M}}^{-1}(\boldsymbol{r}) \times \frac{1}{k_{eff}^{(n-1)}} \overline{\overline{F}}(\boldsymbol{r}) \times \bar{\phi}^{(n-1)}(\boldsymbol{r}) \tag{18}$$

and

$$k_{eff}^{(n)} = \frac{\overline{\overline{F}}(\boldsymbol{r}) \times \bar{\phi}^{(n)}(\boldsymbol{r})}{\overline{\overline{F}}(\boldsymbol{r}) \times \bar{\phi}^{(n-1)}(\boldsymbol{r})} \times k_{eff}^{(n-1)} \tag{19}$$

where (n) represents the iteration number. The starting point of this method is an initial guess for $\bar{\phi}^{(0)}(\boldsymbol{r})$ and $k_{eff}^{(0)}$. In this study, the values given by SIMULATE-3 were chosen[1]. Then, a new flux distribution is calculated via Eq. (18), and subsequently a new eigenvalue is estimated via Eq. (19). This procedure is repeated until some convergence criteria regarding both the neutron flux and the eigenvalue are fulfilled. Then the results have to be scaled since Eq. (10) is a homogeneous equation. The scaling is required for comparison purposes between the static core simulator and SIMULATE-3. The scaling factor is calculated so that the power level corresponds to the one given by SIMULATE-3 in the axially condensed reactor:

$$\int_{fuel} [\kappa_1(\boldsymbol{r})\phi_1(\boldsymbol{r}) + \kappa_2(\boldsymbol{r})\phi_2(\boldsymbol{r})]d\boldsymbol{r}\Big|_{\text{static core simulator}} = \int_{fuel} [\kappa_1(\boldsymbol{r})\phi_1(\boldsymbol{r}) + \kappa_2(\boldsymbol{r})\phi_2(\boldsymbol{r})]d\boldsymbol{r}\Big|_{\text{SIMULATE-3}} \tag{20}$$

where $\kappa_1(\boldsymbol{r})$ and $\kappa_2(\boldsymbol{r})$ are the energy release per fast and thermal fission respectively.

This static core simulator was then benchmarked against SIMULATE-3. In such a benchmark, the cross-sections used in the 2-D simulator were obviously obtained directly from the 3-D core modelled in SIMULATE-3 without any modification of the absorption cross-sections (which would have been necessary to take the leakage in the axial direction into account, as described previously (see Section 1.2)). Such a cross-section adjustment would have made the axially condensed systems significantly different with respect to the flux calculation. It is therefore expected that the eigenvalue given by the static core simulator (2-D system) will be significantly larger than the one given by SIMULATE-3 (3-D system).

The results of the benchmarking are given in Figs. 1 - 3. The peaks observed in Fig. 2 correspond to the reflector peaks, i.e. an increase of the thermal flux in the reflector region, and are observed both in the SIMULATE-3 results and in the results of the 2-D 2-group static core simulator. Furthermore, the agreement between the static core simulator and SIMULATE-3 is very good in the fuel zone. The discrepancy is nevertheless relatively

1. For the flux, the axially condensed flux given by SIMULATE-3 is actually used.

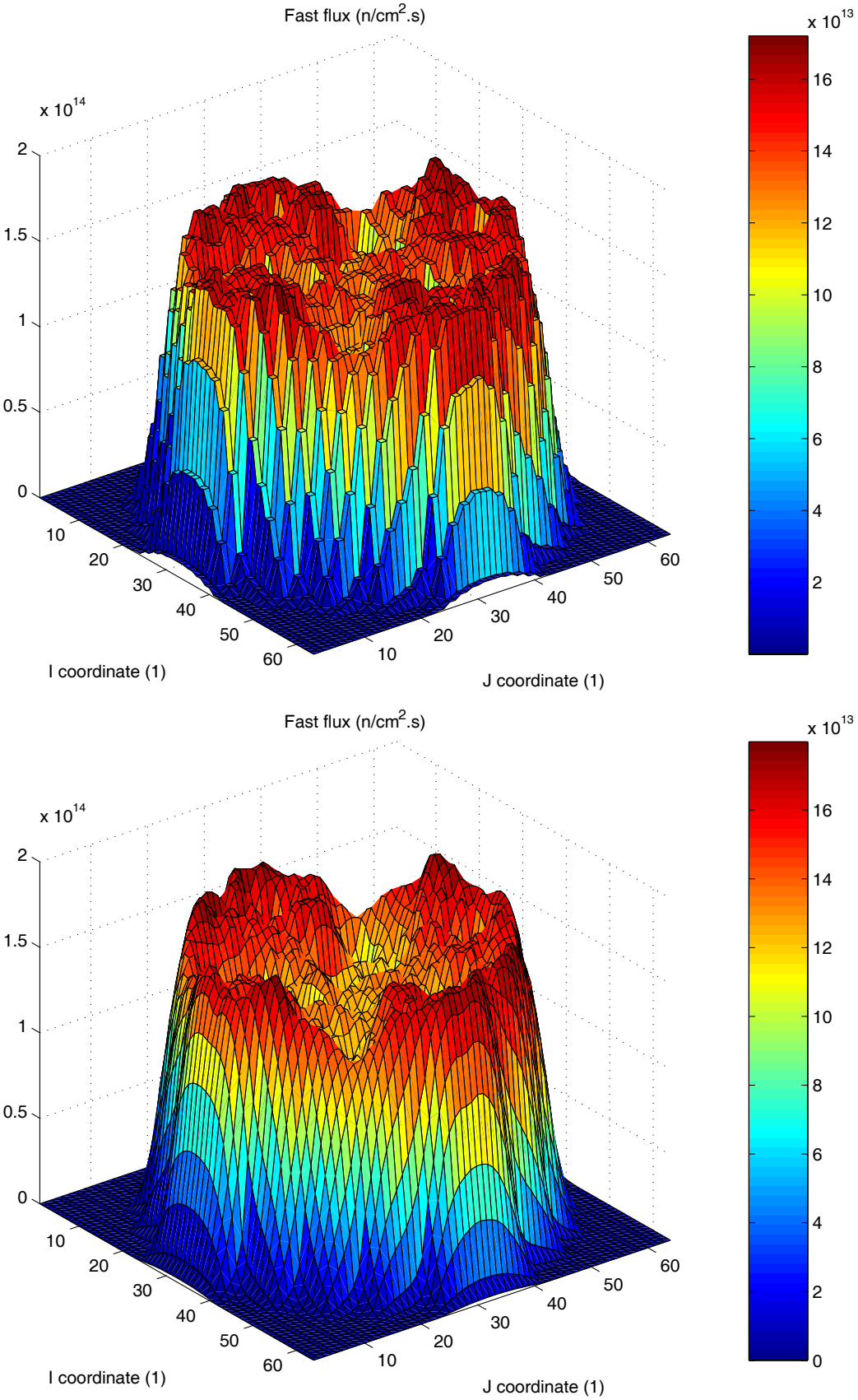

Fig. 1. *Static flux calculations in the fast group (the reference solution given by SIMULATE-3 is given in the upper figure, and the solution calculated by the 2-D 2-group static core simulator is given in the lower figure)*

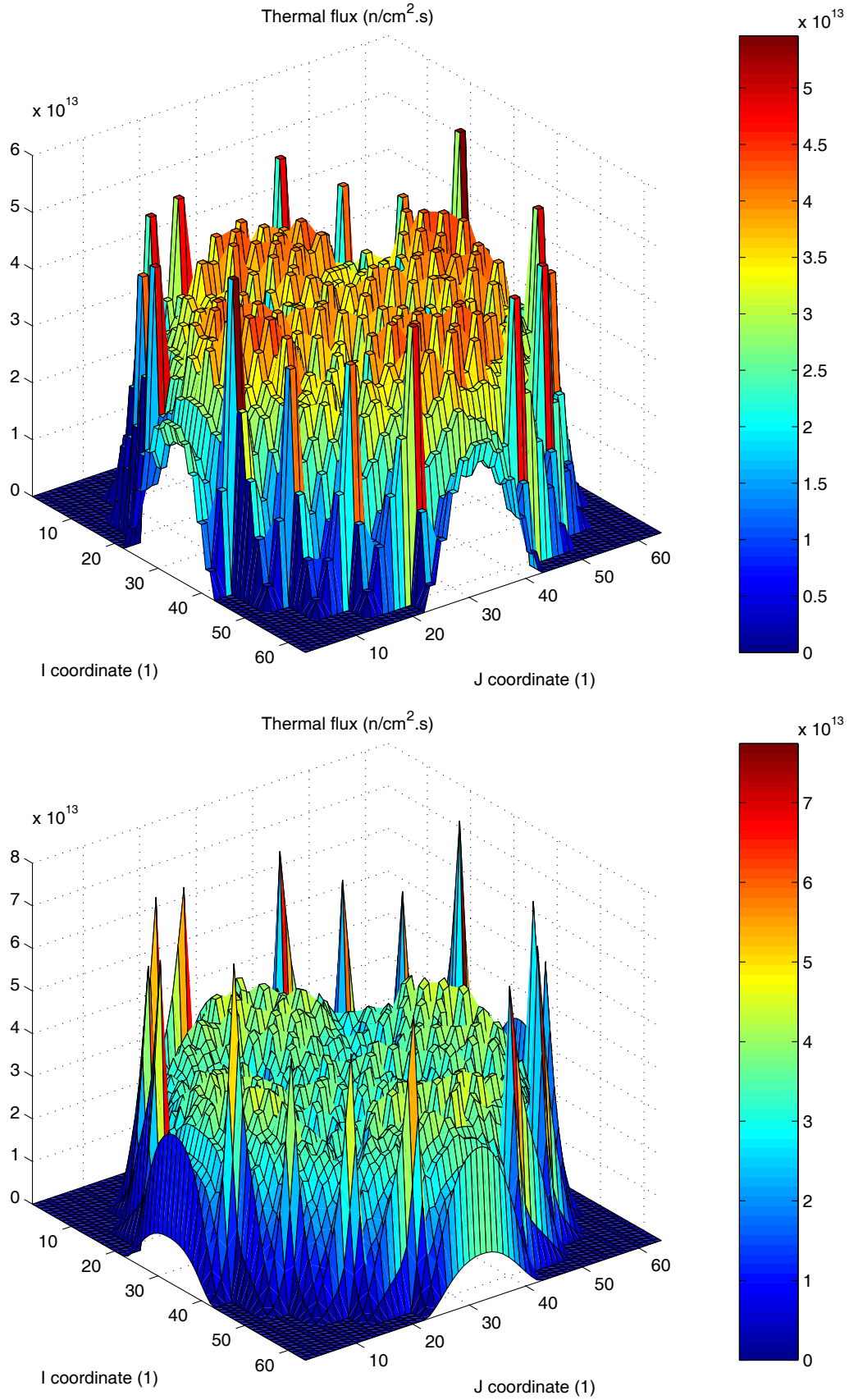

Fig. 2. *Static flux calculations in the thermal group (the reference solution given by SIMULATE-3 is given in the upper figure, and the solution calculated by the 2-D 2-group static core simulator is given in the lower figure)*

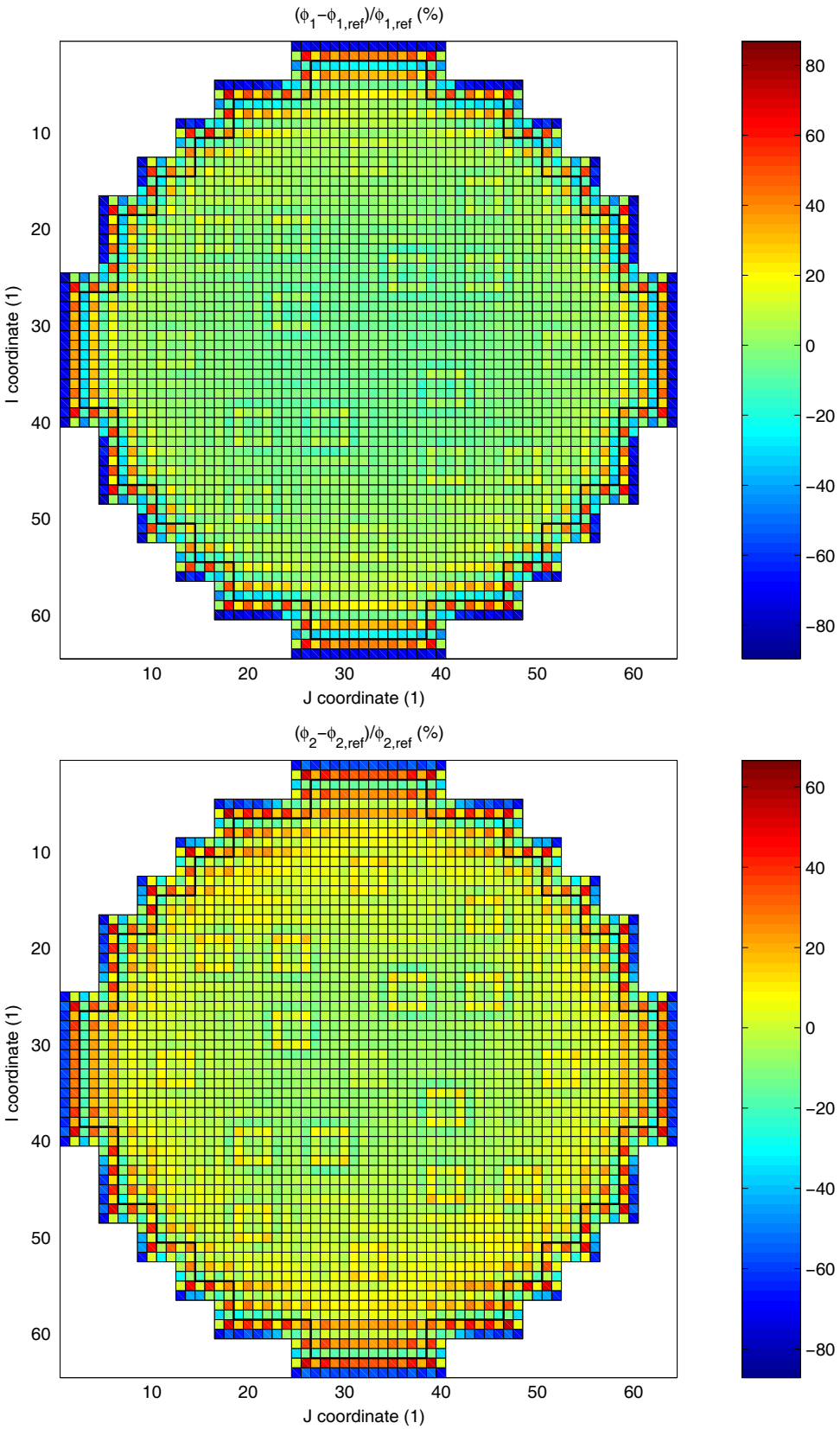

Fig. 3. *Relative difference in the static flux calculations between the static core simulator and SIMULATE-3 in the benchmark case, with SIMULATE-3 being considered as the reference case; the comparison of the fast flux is given in the upper figure, and the comparison of the thermal flux is given in the lower one*

significant in the reflector zone for two main reasons. First of all, the discretisation scheme used in the static core simulator, i.e. the finite difference scheme, is known to give poor results when there are large flux gradients, such as for instance in the reflector region and close to this region. SIMULATE-3 uses a nodal diffusion model, which gives much more accurate results in such cases. Another difference between the two modelling is the number of nodes used in the calculation. In SIMULATE-3, the core is described via a 32x32 lattice, whereas the static core simulator uses a 64x64 lattice. In order to compare the results of the two calculations, the SIMULATE-3 results were simply expanded on the 64x64 grid without any interpolation, i.e. the results are spatially homogeneous on each 2x2 node. Consequently, a reflector "assembly" is actually described by 2x2 nodes in the static core simulator, whereas it is described by only 1x1 node in SIMULATE-3. Since the static flux is assumed to vanish at the core boundary, big discrepancies are thus expected in the reflector region. Concerning the eigenvalue calculation, the static core simulator gives a value of 1.00649, whereas SIMULATE-3 gives a value of 1.00425. This discrepancy was expected since the static core simulator represents a 2-D system in which the axial leakage was eliminated, whereas SIMULATE-3 represents an actual 3-D system.

1.4 Application of the localisation algorithm to the Forsmark-1 instability event

With the improvements described previously, the anomaly localisation procedure was applied to the Forsmark-1 channel instability event recorded in January 1997, during the fuel cycle 16. The algorithm used for that localisation is completely identical to the one used in [7], the only differences are the set of cross-sections and point-kinetic parameters of the core (which correspond to the Forsmark-1 core) and the set of the static fluxes (which were calculated by using a 2-D 2-group static core simulator compatible with the neutron noise simulator). This means that the reactor transfer function used to perform the localisation is more realistic than the one used previously in [7], and consequently one might expect a more reliable location of the noise source in the Forsmark-1 case.

The results of the new localisation are depicted in Fig. 4. As a matter of fact, the function calculated by the localisation procedure is depicted in 3-D and in 2-D. The minimum of this function corresponds to the location of the noise source. In this Figure, the detectors that were used in the localisation search are represented by white crosses, whereas the detectors that were not used are represented by black crosses. The noise source pointed out by the localisation algorithm is very close to a fuel assembly which was discovered to be unseated during the fuel outage following the fuel cycle 16. As already explained in [7], an unseated fuel assembly renders the fuel channel thermal-hydraulically unstable (Density Wave Oscillation or DWO), and this corresponds to an "absorber of variable strength" type of noise source, which is the type of noise source that the neutron noise simulator is able to model.

If one compares these new results with the results presented in Stage 7, one notices immediately that the noise source pointed out this time by the algorithm is closer to the unseated fuel assembly than in Stage 7. Furthermore, using the three detectors surrounding the unseated fuel assembly was good enough to correctly locate the noise source, whereas in Stage 7 it was necessary to use five detectors. Furthermore, in Stage 7 the minimum of the function calculated by the algorithm was found in the reflector region. This global minimum was therefore disregarded, and a local minimum was found in the fuel region. With the new reactor transfer function used in this study, the global minimum was directly found in the fuel region, and very close to the unseated fuel assembly.

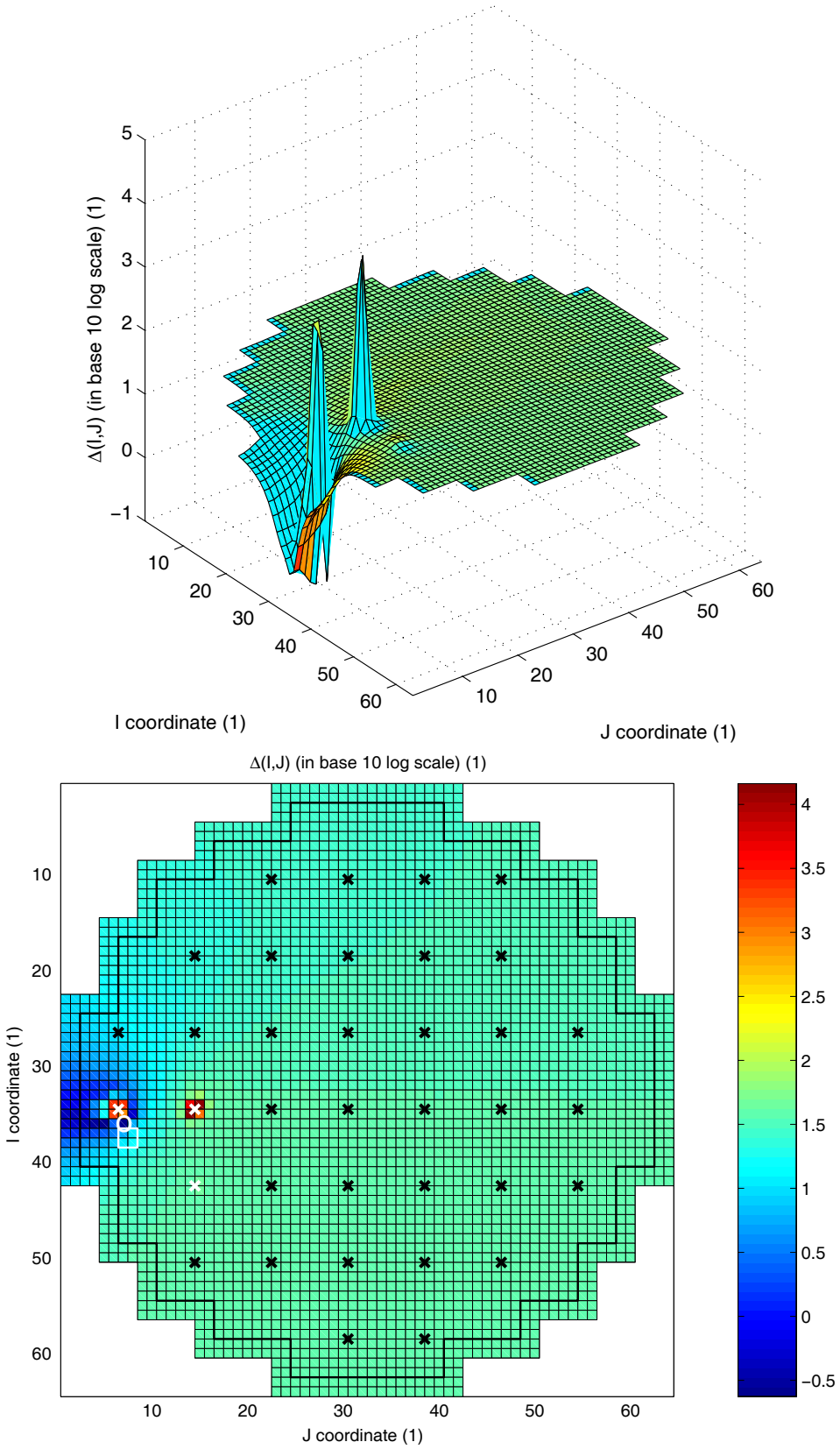

Fig. 4. *Result of the localisation algorithm in the Forsmark-1 case (local instability event); the unseated fuel element is marked with a square, and the noise source identified by the localisation algorithm with a circle. The detectors that were used in the localisation search are marked by white crosses, whereas the detectors that were not used are marked by black crosses.*

As was suggested in Stage 7 and as can be seen also in Fig. 5, using all the available detector signals seems to indicate that at least two noise sources coexist at the same time in the core. As before, the detectors that were used in the localisation search are represented by white crosses, whereas the detectors that were not used are represented by black crosses. As explained in Stage 7, the location of the noise sources is biased if there are several noise sources in the core, since the localisation procedure was developed to handle only one noise source at a time. It was also demonstrated in Stage 7 that using a reduced set of detectors, the detectors surrounding one of the noise sources, allows correctly locating this specific noise source, as illustrated previously in Fig. 4. Although the noise sources pointed out in Fig. 5 might be misplaced, this Figure confirms that more than one noise source was present in the Forsmark-1 case. Furthermore, as explained in the following Section 2, the presence of one single noise source does not allow explaining a strongly space-dependent Decay Ratio (DR), as was observed in Forsmark-1.

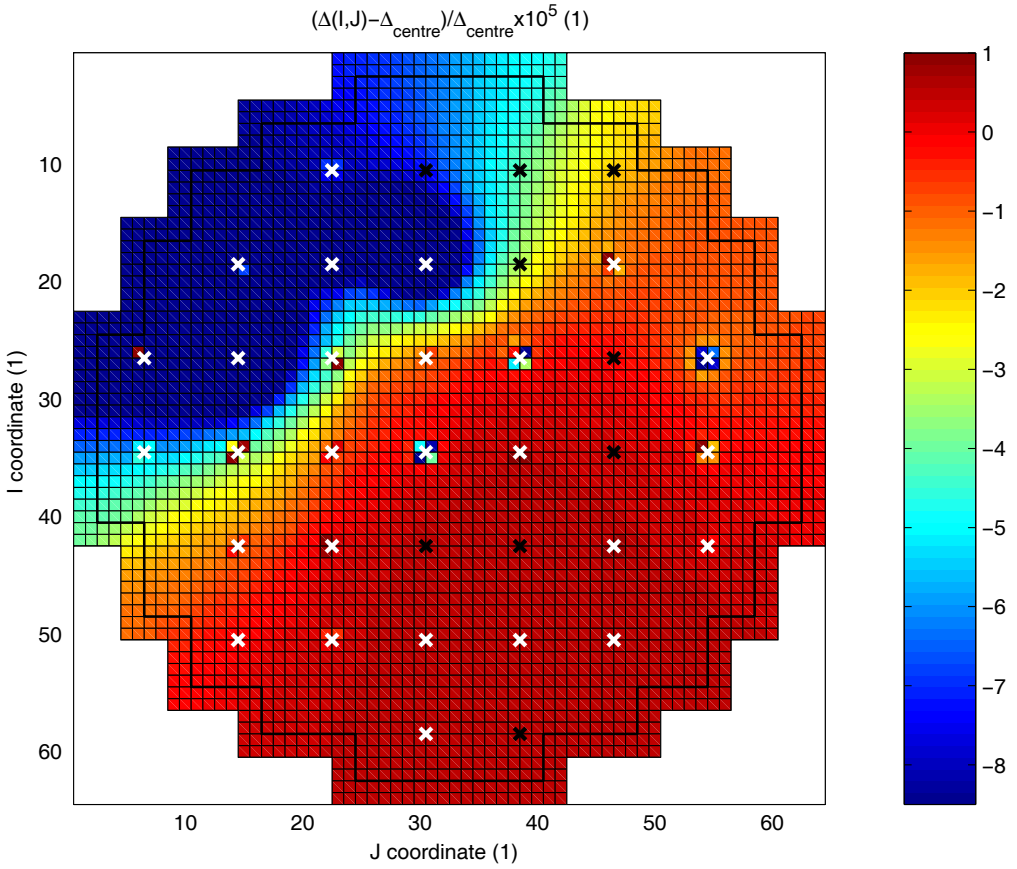

Fig. 5. *Result of the localisation algorithm in the Forsmark-1 case (local instability event) when all the available detector signals are used*

1.5 Conclusions

In this Stage, a static core simulator was developed in order to be used with the neutron noise simulator. As a matter of fact, an adjoint core simulator was also developed [11], since the calculations of the direct and adjoint fluxes are two equivalent tasks. This consequently means that the Department of Reactor Physics has now a full package to perform 2-D core calculations in the 2-group diffusion approximation: a static core simulator, an adjoint core simulator, and a neutron noise simulator. In order to use the

neutron noise simulator, the static core simulator has first to be used so that the direct fluxes and the corresponding eigenvalue can be calculated with a discretisation scheme compatible with the neutron noise simulator. The only data required to use these codes are thus the 2-D 2-group material constants (and the point-kinetic parameters of the core for the neutron noise simulator).

With this new package and a new set of data representative of the Forsmark-1 reactor corresponding to the channel instability event recorded in January 1997 during the fuel cycle 16, the localisation algorithm developed previously in Stage 7 was again used. Using a reduced set of detectors showed that the noise source pointed out by the algorithm was very close to an unseated fuel assembly. It was also demonstrated in this Stage that the more realistic reactor transfer function allowed improving significantly the results of the search procedure (noise source closer to the unseated fuel assembly than in Stage 7, only three detectors required to get a successful noise source localisation, and location of the noise source directly given by the global minimum of the function estimated by the localisation algorithm). It was also demonstrated by using all the available detector signals that the presence of at least two noise sources in the Forsmark-1 case was highly possible. Such an hypothesis is reinforced in the next Section, which investigates one of the possible reasons why the DR in the Forsmark-1 case is strongly spatially-dependent, namely the fact that several types or sources of instability were simultaneously present in the core.

Section 2

A phenomenological model for the explanation of a strongly space-dependent Decay Ratio

2.1 Introduction

During a measurement campaign performed during the fuel cycle 16 in the Forsmark-1 Boiling Water Reactor (BWR) in order to study BWR stability, it was noticed that the so-called Decay Ratio (DR) was strongly radially space-dependent [12]. The DR, which characterises the stability of a BWR, has previously always been assumed to be a space-independent parameter of the core. This space-dependent character of the DR could not be understood.

A phenomenological model suggested by Pázsit in [13] was applied to the Forsmark-1 case. Originally, this model was derived to explain the discontinuous character of the DR when the operating point was changed smoothly on the power-flow map. Such a behaviour was found in the Swedish BWR Ringhals-1, where dual oscillations (local and regional) appeared simultaneously. In the study reported in [13], the space dependence of the decay ratio was not investigated, only its dependence on the operating point. However, the model takes into account the space dependence of the different oscillations, hence it was used in this study to show that the coexistence of two types or sources of instability with different DRs and space dependence can make the DR strongly space-dependent. Two cases were investigated in this study: the case of a local noise source coexisting with a global noise source (in-phase oscillations), and the case of two local noise sources. In order to use this phenomenological model in these two cases, the calculation of the spatial structure of the neutron noise induced by the aforementioned noise sources is required.

In the following, the Forsmark-1 measurement is first described in detail. The different models used to estimate theoretically the DR are thus explained. Then, the space-dependence of the DR is estimated from the phenomenological model and compared to the measured DR.

2.2 Description of the Forsmark-1 case

In 1996, during the start-up tests of the Forsmark-1 BWR for the fuel cycle 16, instability conditions were detected at reduced power and reduced core-flow. Forsmark-1 is a BWR of the Westinghouse Atom design (previously ABB Atom AB, or ASEA-Atom AB) built in 1980 and has a thermal core-rated power of 2700 MWth and a nominal core flow of 10450 kg/s. Although BWRs are known to become less stable at reduced power/core flow, the appearance of this instability could not be understood and was not predicted by the stability calculations. The corresponding operating point in the power/flow map was therefore avoided. In January 1997, at approximately Middle Of Cycle conditions (MOC), stability measurements were carried out in order to study the instability discovered previously. The core was thus brought to 63.3% of power and to a core flow of 4298 kg/s. Again instability conditions were encountered, at a frequency of roughly 0.5 Hz.

During this stability measurement the lower plane of the core was rather well equipped with Local Power Range Monitors (LPRMs), where signals from 27 of the 36 available detector strings were actually recorded at a sampling frequency of 12.5 Hz. One parameter that is relevant for characterizing the stability of BWRs is the DR, which is defined as the

ratio between two consecutive maxima A_i and A_{i+1} of the Auto-Correlation Function (ACF) of the normalized neutron density, or alternatively two consecutive maxima of the Impulse Response Function (IRF) as calculated by using an Autoregressive Moving-Average (ARMA) or an Autoregressive model (AR) to fit the behaviour of the system. These methods are illustrated in Fig. 6. The DR gives therefore a measure of the inherent damping properties of the system. Using each detector separately allows estimating the Decay Ratio (DR) according to the following standard method [14]:

$$DR = \frac{A_{i+1}}{A_i}, \qquad \forall i \tag{21}$$

Although the DR was always assumed to be a 0-D parameter of the core, i.e. independent of the position where the DR is estimated in the core, the Forsmark-1 measurement revealed that the DR was actually strongly space-dependent, as can be seen on the following Fig. 7. This Figure shows that one half of the core exhibits a DR close to instability (higher than 0.9) and the other half has a DR close to 0.6.

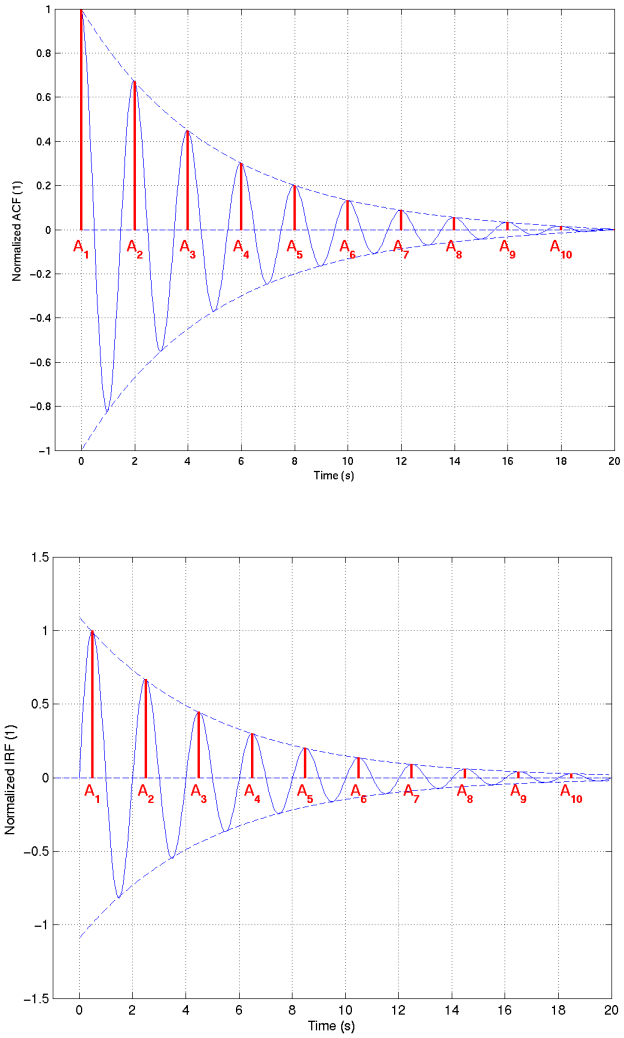

Fig. 6. *ACF and IRF of a second-order system (on the upper figure and the lower figure respectively).*

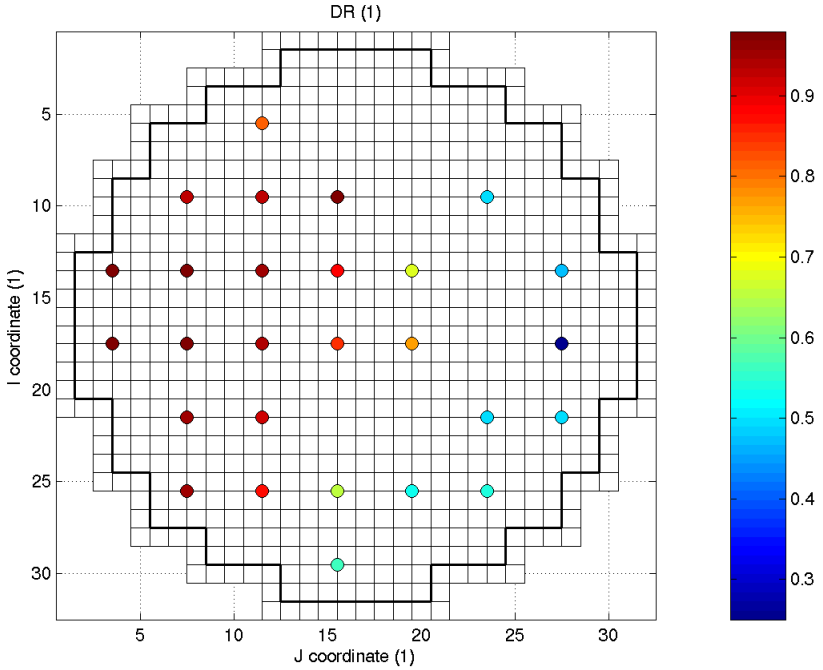

Fig. 7. *Measured radial space-dependence of the Decay Ratio in Forsmark-1 (derived from [15])*

A closer look at the phase of the measured flux noise indicated that the neutron noise was driven by a local noise source, similar to the effect of an absorber of variable strength (reactor oscillator). As a matter of fact, more detailed analyses of this instability event revealed that the reason of this instability was due to the presence of one or more likely two noise sources (see [16], [17], and Section 1). In these aforementioned analyses, even a localisation of these noise sources was carried out, and one of the noise sources pointed out by the localisation algorithm was close to a fuel assembly which was found to be unseated during the fuel outage following the fuel cycle 16. As pointed out by [18], when a fuel element is unseated, some of the coolant flow bypasses the fuel element and this might render the channel thermal-hydraulically unstable (self-sustained Density Wave Oscillation or DWO [19]).

2.3 Description of the models and calculation of the noise

The fact that the observed DR in the Forsmark-1 case exhibits a strong space-dependence suggests that two types or sources of instability are present at the same time in the core. If there was only one type or one source of instability, the DR would not be space-dependent, and would roughly be the same whatever LPRM is used to perform the DR evaluation. In the following, an analytical model that allows estimating the DR resulting from two types/sources of instability is presented and its application to the Forsmark-1 case is explained.

The analytical model

The analytical model to calculate the DR in case of dual oscillations will be taken from an earlier work of Pázsit [13]. This model was developed to explain the discontinuous

character of the DR when the operating point was changed smoothly on the power-flow map, and relied on dual oscillations according to which the DR was calculated. Although the model is rather simple in order to make analytical calculations possible with the goal of expediting insight and understanding, its domain of validity was confirmed also in detailed core calculational models [20]. The same model will be used in this paper to study the space-dependence of the DR. The only difference compared to the previous investigation is the type or source of instability investigated. In [13], only the case of a regional (out-of-phase) type of oscillation coexisting with a global (in-phase) type of oscillation was investigated. This model was extended here to any type or source of instability existing simultaneously in the core. More specifically, two cases are presented: the case of a local noise source coexisting with a global type of oscillation, and the case of two local noise sources. In the following, the main characteristics of the model proposed in [13] are recalled.

The starting point is to write that the flux fluctuations can be written as a sum between the contribution of two noise sources, each of them being factorized into a temporal part only and a spatial part only as follows:

$$\delta\phi(\boldsymbol{r}, t) = \delta\phi_1(\boldsymbol{r}, t) + \delta\phi_2(\boldsymbol{r}, t) = \delta\psi_1(t)\varphi_1(\boldsymbol{r}) + \delta\psi_2(t)\varphi_2(\boldsymbol{r}) \tag{22}$$

where the amplitudes $\delta\psi_i(t)$ (i=1, 2) are second-order processes, with the same resonance frequency ω_0, but different damping properties. As will be shown later, for the case of local instability, the factorisation does not hold in a strict sense; nevertheless, it is quite well applicable in the frequency range considered. At any rate, this study relies on this basic assumption. If one further assumes that the aforementioned second-order processes are driven by the driving forces $f_i(t)$ (i=1, 2), the amplitudes $\delta\psi_i(t)$ (i=1, 2) will obey the following equation:

$$\delta\ddot{\psi}_i(t) + 2\xi_i\omega_0\delta\dot{\psi}_i(t) + \omega_0^2\delta\psi_i(t) = f_i(t) \tag{23}$$

For simplicity, we will neglect the cross-term between the two noise sources, i.e. we will assume that:

$$CPSD_{f_1 f_2}(\omega) = CPSD_{f_2 f_1} \approx 0 \tag{24}$$

If one further assumes that the DR of any of the two types or sources of instability is larger than 0.4, the second-order terms in ξ can be neglected, and it was shown in [13] that the ACF of any LPRM signal can then be given by:

$$ACF(\boldsymbol{r}, \tau) = \cos(\omega_0\tau) \sum_{i=1}^{2} a_i(\boldsymbol{r}) \cdot e^{-\xi_i\omega_0\tau} \tag{25}$$

with

$$a_i(\boldsymbol{r}) = \frac{1}{1 + \dfrac{APSD_{f_j}}{APSD_{f_i}} \dfrac{\varphi_j(\boldsymbol{r})}{\varphi_i(\boldsymbol{r})} \dfrac{\ln(DR_i)}{\ln(DR_j)}}; \qquad j \neq i \tag{26}$$

Eq. (25) does not correspond to a pure second-order system, and therefore the definition of its DR is not unique. From a measurement viewpoint, it is practical to define the DR as the ratio between the first and the second maxima of the ACF, i.e.:

$$DR(\boldsymbol{r}) = \sum_{i=1}^{2} a_i(\boldsymbol{r}) \cdot e^{-2\pi\xi_i} \tag{27}$$

where

$$DR_i = e^{-2\pi\xi_i} \tag{28}$$

As is explained in [13], the cross-term can be explicitly accounted for. In such a case the expressions that we would obtain would be more complicated, but the model of the DR presented previously would be essentially the same, only the weighting coefficient $a_i(\boldsymbol{r})$ between the two types or sources of instability would be different. Furthermore, Eq. (28) allows verifying the other hypothesis used in this model, i.e. that neglecting ξ^2 besides unity is justified for any DR larger than 0.4.

Evaluation of the spatial components

In order to calculate the space-dependence of the DR when two types or sources of instability coexist in the core, one needs to estimate the coefficients $a_i(\boldsymbol{r})$ used in Eq. (27), i.e. one needs to define the f_i parameters and to calculate the functions $\varphi_i(\boldsymbol{r})$. The f_i parameters (or more exactly their ratio) can be chosen freely. The functions $\varphi_i(\boldsymbol{r})$, which represent the spatial dependence of the induced neutron noise, depend on the type or source of instability.

In case of a global-type of oscillations, it is well known that the induced neutron noise is spatially distributed according to the static flux $\phi_0(\boldsymbol{r})$, i.e. is given in the frequency domain by:

$$\delta\phi(\boldsymbol{r}, \omega) = \phi_0(\boldsymbol{r}) G_0(\omega) \delta\rho(\omega) \tag{29}$$

where $G_0(\omega)$ and $\delta\rho(\omega)$, are the zero-power reactor transfer function and the reactivity noise (noise source) respectively, so that:

$$\varphi_i(\boldsymbol{r}) = C_i \phi_0(\boldsymbol{r}) \tag{30}$$

where C_i is a scaling coefficient.

In case of a local noise source, the induced neutron noise is given in the frequency domain by:

$$\delta\phi(\boldsymbol{r}, \omega) = G(\boldsymbol{r}, \boldsymbol{r}_0, \omega) S_{r_0}(\omega) \tag{31}$$

where $S_{r_0}(\omega)$ and $G(\boldsymbol{r}, \boldsymbol{r}_0, \omega)$ are the noise source localised at the position $\boldsymbol{r}_0$ and the corresponding Green's function (transfer function) of the noise equations, respectively [16]. Eq. (31) shows that, in general, for the local oscillations, the space and frequency (or space

and time) dependence of the neutron fluctuations does not factorise. However, one can make use of the fact that the transfer function $G(\boldsymbol{r}, \boldsymbol{r}_0, \omega)$ depends on frequency only through the zero-power reactor transfer function $G_0(\omega)$. This latter, on the other hand, depends very weekly on the frequency in the so-called plateau region, roughly between 0.05 and 15 Hz. Since the oscillation frequency of the local instability was about 0.5 Hz, one can use the values of $G(\boldsymbol{r}, \boldsymbol{r}_0, \omega)$ at the resonance frequency ω_0. Hence, one can write:

$$\varphi_j(\boldsymbol{r}) = C_j \left| G(\boldsymbol{r}, \boldsymbol{r}_0, \omega_0) \right| \tag{32}$$

where C_j is another scaling factor. Since it is only the ratio of the scaling factors in Eqs. (30) and (32) that counts, we shall assume $C_j = 1$ in Eq. (32).

Consequently, one needs to estimate both the static flux and the neutron noise induced by the localised noise source(s) in order to use the phenomenological model given by Eqs. (26) and (27). Since this study investigates the case of the Forsmark-1 BWR, i.e. a strongly heterogeneous core, the static flux was calculated by a 2-D 2-group static core simulator and the neutron noise by a 2-D 2-group noise simulator. The properties, and the functioning of these simulators are described in detail in Section 1 of this report and in [7].

2.4 Results

In the following, the results of the previous phenomenological model applied to Forsmark-1 are presented. Two cases are investigated: the case of a local noise source coexisting with a global noise source, and the case of two local noise sources.

The case of a local noise source and a global noise source

The results corresponding to the case of a local noise source coexisting with a global noise source (in-phase oscillations) are presented in Fig. 8. The DR corresponding to the local noise source was set to 0.99, whereas the DR corresponding to the in-phase oscillations was set to 0.4. The local noise source was located at the position pointed out by a noise source localization algorithm applied previously in [17] to the case of the Forsmark-1 channel instability event. Finally, as explained earlier, the ratio f_2 / f_1 can be chosen freely and was determined so that the DR calculated throughout the core matched the measured DR. As can be seen on Fig. 8., the DR calculated by using the phenomenological model given by Eqs.(26) and (27) in case of a local noise source and a global noise source is strongly spatially dependent, and reproduces quite well the behavior of the measured DR in Forsmark-1.

The reason for the relatively sharp boundary between the two values of the DR is the fast spatial decay of the local oscillations. Thus there are two different regions in the core, one in which the local oscillations dominate, and one in which the global ones dominate, with a relatively narrow transition region. Such a case would not occur with concurrent global and regional oscillations, only when at least one local component is involved.

The case of two local noise sources

The results corresponding to the case of two local noise sources are presented in Fig. 9. The local noise source with a DR of 0.99 was located at the position pointed out by the noise source localization algorithm applied previously in [17] to the case of the Forsmark-1

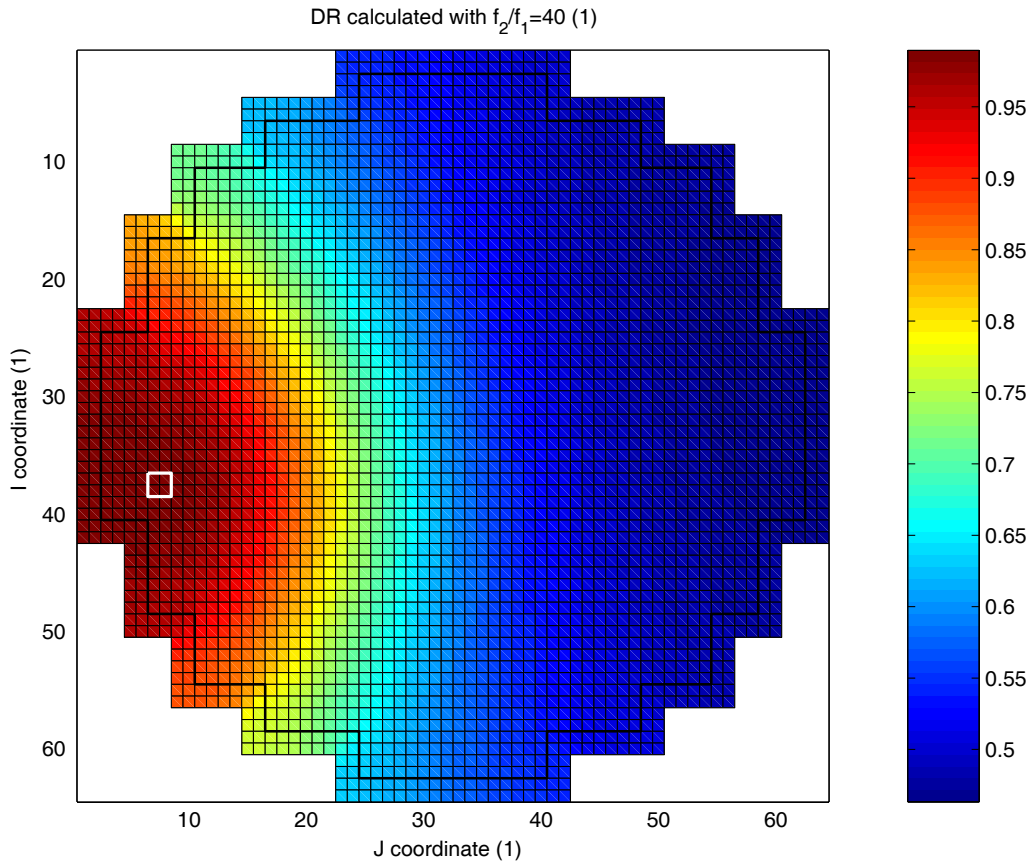

Fig. 8. *Simulated radial space-dependence of the Decay Ratio in Forsmark-1 in case of a local noise source and a global noise source (the white square represents the location of the local noise source).*

channel instability event. The noise source with a DR of 0.4 was positioned on the opposite side from the other noise source. The ratio was chosen so that the DR calculated throughout the core matched the measured DR. As can be seen on Fig. 9., the DR calculated by using the phenomenological model given by Eqs. (26) and (27) in case of two local noise sources is strongly spatially dependent, and reproduces again rather well the behavior of the measured DR in Forsmark-1. Again, the reason of the sharp boundary between the two stability regions is the fast spatial decay of the amplitude of the local oscillations.

2.5 Conclusions

The purpose of this paper was to construct a simple model, with the help of which the experimentally found space-dependence of the Decay Ratio (DR) is possible. In the early cases of BWR instability, the DR appeared to be a space-independent parameter of a BWR core, characterizing its global stability. Nevertheless, it was noticed during the Forsmark-1 channel instability event (January 1997) that the DR measured throughout the core using LPRM signals was radially strongly space-dependent, ranging from 0.6 on the right-hand side of the core to values higher than 0.9 on the left-hand side of the core, i.e. values close to limit-cycle oscillations.

The phenomenological model of the DR developed by Pázsit in [13] was used in this paper in order to calculate the space-dependence of the DR in case of several types or sources of instability, each of them having different stability properties and space dependence. More specifically, two cases were investigated: a local noise source coexisting

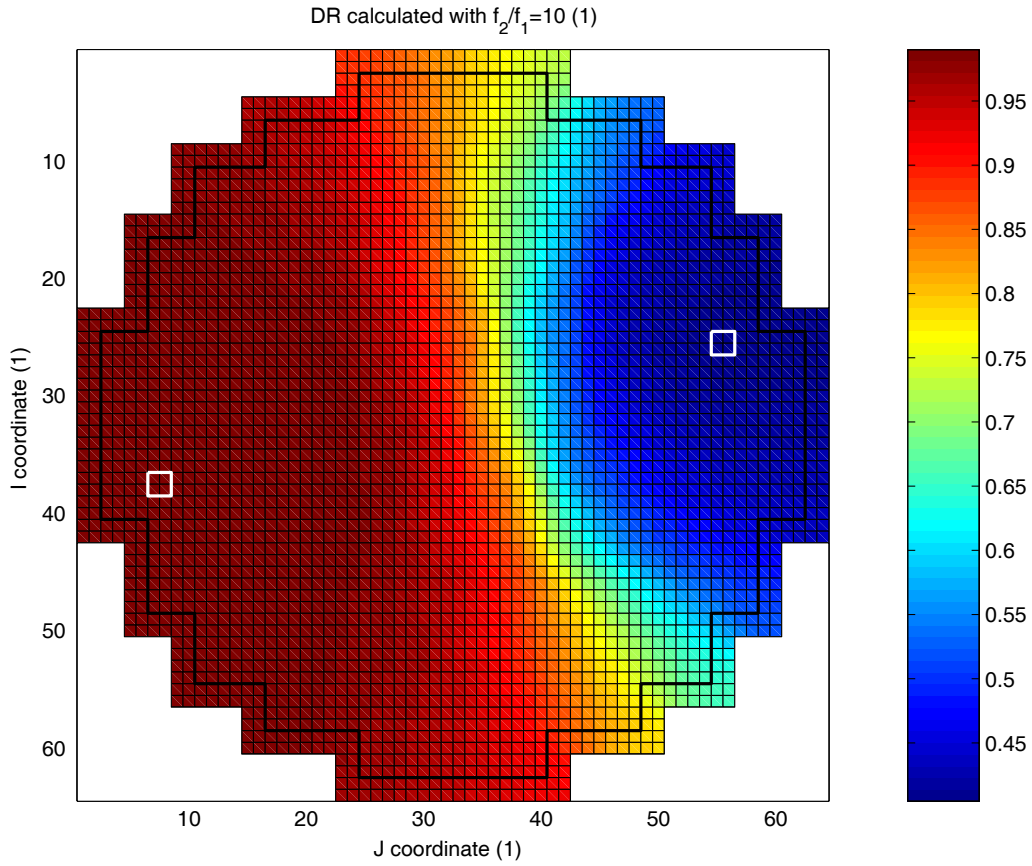

Fig. 9. *Simulated radial space-dependence of the Decay Ratio in Forsmark-1 in case of two local noise sources (the white squares represent the location of the local noise sources).*

with a global noise source (in-phase oscillations), and two local noise sources. It was shown, via the use of a 2-D 2-group static core simulator and a 2-D 2-group neutron noise simulator applied to realistic data corresponding to the Forsmark-1 instability event, that the space-dependent character of the measured DR could be reproduced. This therefore confirms our original idea that in case of dual oscillations with different space-dependence, i.e. when several types or sources of instability coexist at the same time in the core, the DR itself becomes necessarily space-dependent. In the case when at least one local oscillation is involved, the DR may appear as discontinuous in space, which is the case that was observed in Forsmark.

Section 3

Continued analysis of the detector impacting with wavelets

3.1 Introduction

As described also in the previous Stage, methods of detecting and quantifying detector tube vibrations, and especially impacting, has been investigated at our Department ([3], [7], [21]-[23]). The interest in this matter stems from the fact that cases of detector string vibrations and impacting have been observed in many BWRs abroad and also in Sweden.

As also described in the previous Stage, [7] most traditionally used methods are not absolute, rather relative and need access to data from the same string before impacting. There is naturally a need for developing an absolute method that does not need calibration to vibration data without impacting from the monitored string. We have some time ago found that wavelet analysis has this potential, and started investigating this potential. The principle of the wavelet based detection is based on the assumption that each impacting event causes a transient in the detector signal which can then be eliminated from the background noise. The performance of the Haar wavelets for this purpose was investigated in earlier work, both with simulated data and with measured data. The measured data analysed in Stage 7 was taken by GSE Power systems, in Oskarshamn-2 between 1991-1994. These data became available to us through an agreement between GSE, SKI and Chalmers. This data basis is ideal for method development because for each measurement the severity of the impacting is known from inspections after refuelling for each fuel cycle.

In Stage 7 only the performance of the Haar wavelet transform was investigated. The investigation of the performance of wavelets other than the Haar wavelet was left for the present Stage. This investigation has now been performed and is the subject of the present Chapter. In the present work, similarly to the previous Stage, the wavelet toolkit of MATLAB was used. Hence, the wavelets available in MATLAB were investigated only in the present work.

Although the primary purpose was to make a comparative analysis of the wavelet set available to us, this work actually contains more. It was understood during the course of the work, that the performance of the wavelet based analysis, done the same way as in the previous Stage, depends very weakly on the type of the wavelets, and instead it depends very strongly on how the analysis (determination of the threshold, the white noise level etc.) was made. We have therefore made a significant further development of the wavelet based methodology and succeeded to decrease the dependence of the method on the number and significance of the freely chosen parameters. In the present form the only input parameter whose value must be specified by the user is the frequency of the hypothetical short transient (the fuel element vibration, induced by the impacting). The rest is a user-independent algorithm.

The performance of this new algorithm was then investigated for the whole MATLAB wavelet set. It turned out that, not only was the new algorithm more effective than the previous one, but also, there was a relatively large variation between the performance of the various wavelets. The most effective wavelets are now more effective than the best non-wavelet based methods. The Chapter gives a description of the algorithm, and gives a thorough comparative analysis of the MATLAB wavelets.

3.2 Physical model of impacting

The physical quantity that allows us to identify mechanical vibrations of a neutron detector is the neutron flux gradient at the detector position. In case of a non-zero gradient, the vibrating detector moves between positions with different neutron flux, thus giving an output signal proportional to the mechanical oscillations. Of course, in reality the detector vibrations are not monochromatic. In practice therefore one applies spectral analysis to the detector signal to find the peak in the APSD function corresponding to the mechanical vibrations. The whole scheme is illustrated in Fig. 10

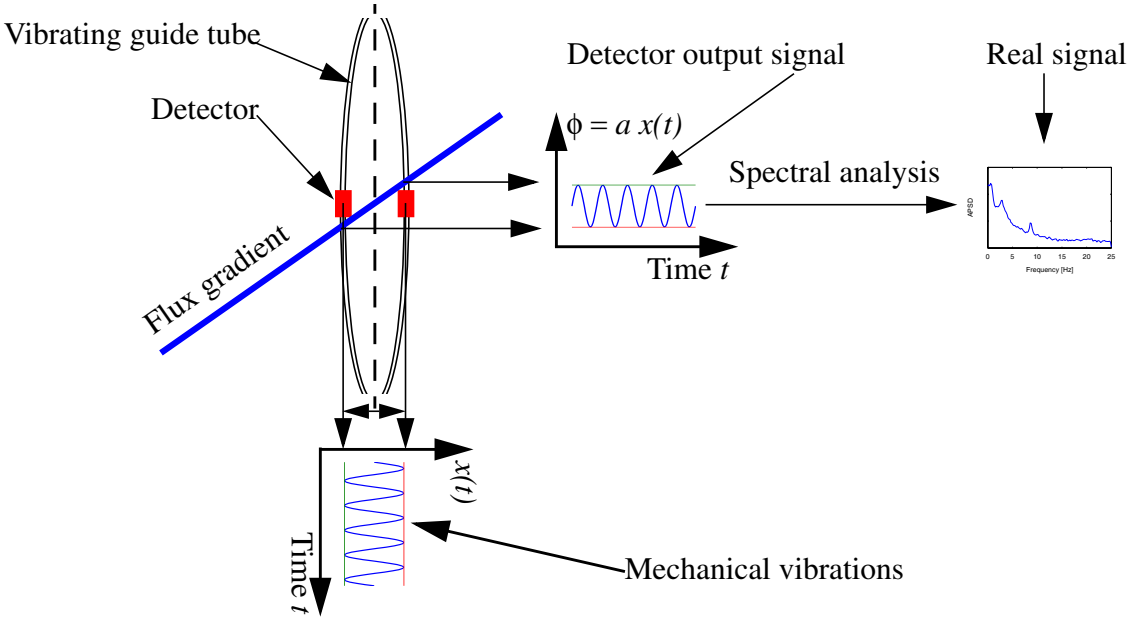

Fig. 10. *Theoretical scheme to detect mechanical vibrations via neutron detectors*

It is worthwhile to notice the following two points. First, the existence of the flux gradient is necessary for obtaining oscillations in the LPRM signals. Otherwise there is no possibility of detecting the vibrations. Nevertheless, in practice the flux gradient is seldom close to zero. Second, usually we do not know the flux gradient and that prevents us from deducing the amplitude of mechanical vibrations via spectral analysis.

The physical model of impacting is based on a suggestion, originally due to Thie, that each impacting of a detector tube against the wall of a fuel assembly will induce short, damped oscillations of the fuel assembly itself, which will contribute to the detector signal. The situation is illustrated in Fig. 11. According to the model we assume the detector signal to consist of:

- a stationary global neutron noise, *N(t)*;
- neutron noise coming from the mechanical vibrations of the detector, *S(t)*, which is additionally supposed to be stationary;
- neutron noise induced by impacting, *T(t)*, which is additionally supposed to be transient.

Summing up the three components we arrive at the following representation for the detector signal.

$$\phi(t) = N(t) + S(t) + T(t) \tag{33}$$

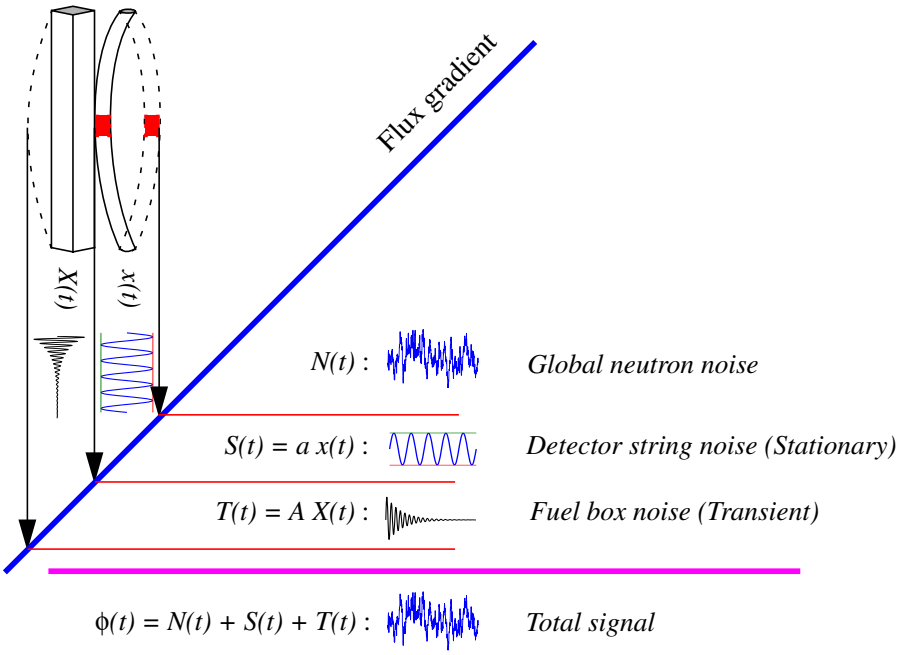

Fig. 11. *Physical model to detect impactings*

3.3 One dimensional model problem

In order to help the developing and testing of the various methods, a simple simulation model was developed. This model was described in previous works ([3], [7]). It is based on the modelling of a one-dimensional damped oscillator, driven by white noise with the governing equation

$$\ddot{x}(t) + 2\theta\dot{x}(t) + \omega_0^2 x(t) \;=\; f(t) \tag{34}$$

with $\langle x(t)\rangle \;=\; 0$ being the equilibrium position, θ standing for the damping factor and *f(t)* being a random driving force. The stochastic force *f(t)* is simulated with a discrete series of impulses. Impacting is simulated by confining the detector string motion within *(-R,+R)*. Whenever $|x(t)|$, in the course of simulation, exceeds *R,* the velocity $\dot{x}(t)$ is reversed, i.e. $\dot{x}(t) \rightarrow -\dot{x}(t)$, which models elastic reflection from an infinite mass without energy loss. Impacting also involves the fuel box vibration that obeys the equation

$$\ddot{X}(t) + 2\Omega\Theta\dot{X}(t) + \Omega_0^2 X(t) \;=\; F(t) \tag{35}$$

where the force *F(t)* is induced by impactings. At each impact, the detector tube transfers a certain impulse, $2m|\dot{x}|$, to the fuel rod. Thus if the box/tube mass ratio is *M/m = k*, then, at impacting, one has $|\dot{X}| \;=\; 2|\dot{x}|/(k+1)$. This will lead to the representation

$$F(t_n) = 2\frac{M}{k+1}\cdot\delta(t-t_n)|\dot{x}(t_n)| \equiv c\cdot\delta(t-t_n)|\dot{x}_n| \tag{36}$$

Finally we assume a linear relationship between the displacement of a fuel box and the induced noise. Thus the neutron noise from a vibrating and impacting detector will be given as

$$\delta\phi(t) = a \cdot x(t) + A \cdot X(t) \tag{37}$$

This model was used also in the present work to generate simulated data for the test of the various algorithms.

3.4 Results with simulated data

The simulation has been performed with the following parameters:

- θ = 2 - damping factor for detector string;
- f_0 = 3.6 - eigenfrequency of detector string;
- Θ = 2 - damping factor for fuel box;
- F_0 = 10 - eigenfrequency of fuel box;
- F = 4 - driving force strength;
- $1/\Delta t$ = 240 - pulse repetition frequency;
- a = 1 - amplitude factor for detector string vibration;
- A = 1 - amplitude factor for fuel box vibration;
- R = 1 - confinement.

Again, these data are the same as the ones used in the previous stage. One example of simulation is shown in Fig. 12 where the upper signal shows the pure detector signal, the second the additional signal induced by the fuel box transient on impacting, and the third plot displays the total detector signal, $\delta\phi(t) = a \cdot x(t) + A \cdot X(t)$. The parameters are chosen such that, like in reality, the fuel box transient is at least 20 times weaker as the detector tube signal, and thus it is completely invisible in the total signal.

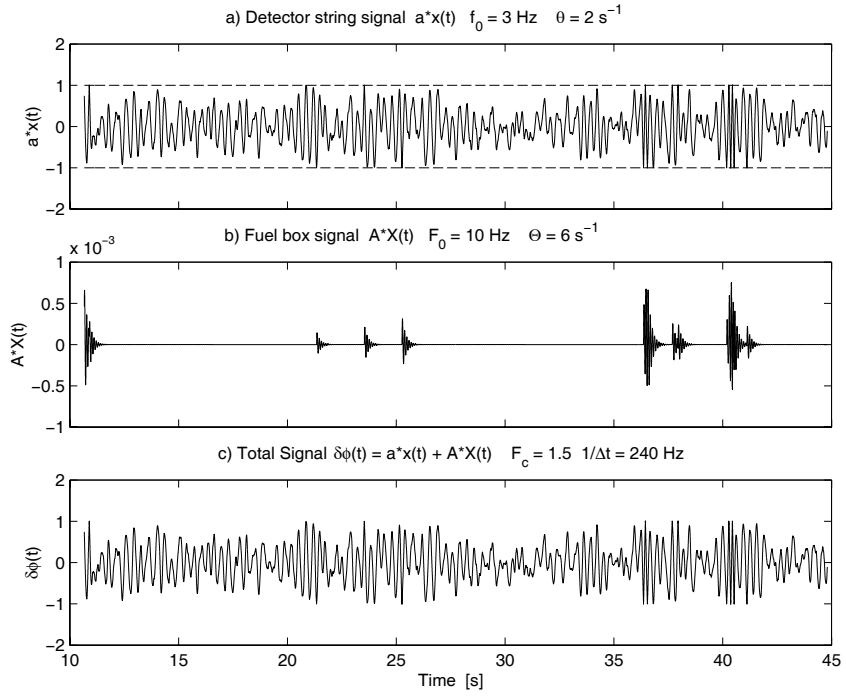

Fig. 12. *Simulated signals*

Fig. 13 presents four wavelets that turn out to be the best in each wavelet family. The selection has been based on analysing the whole wavelet bank available in MATLAB Wavelet Tool Box 2.2. In the course of analysis the simulated signal was studied by using the third-level decomposition $S(t) = A_3(t) + D_1(t) + D_2(t) + D_3(t)$ for each wavelet. The performance of each wavelet is evaluated by visual inspection of the corresponding plots as well as by studying two parameters: details-to-signal ratio, *rDS*, and details-to-details ratio, *rDD*. To introduce these quantities we define first two variants of the mean value and the spread of a signal *S*:

$$\mu = \mu(S) = \frac{1}{N}\sum_{i=1}^{N} S_i \qquad \sigma = \sigma(S) = \sqrt{\frac{1}{N-1}\sum_{i=1}^{N}(S_i - \mu)^2}$$
$$\mu' = \mu'(S) = med(S) \qquad \sigma' = \sigma'(S) = med(|S - \mu'|) \tag{38}$$

Here *med(S)* is the MATLAB function `median` that divides the signal components S_i into two equal parts. Then *rDS* and *rDD* read as

$$rDS = \frac{\sigma'(D_1)}{\sigma'(S)} \qquad rDD = \frac{\sigma'(D_1)}{\sigma(S)} \tag{39}$$

rDS shows the noise content in the signal as evaluated by a certain wavelet, whereas *rDD* gives the ratio of spikes to the average spread of the signal. The less the ratio the better

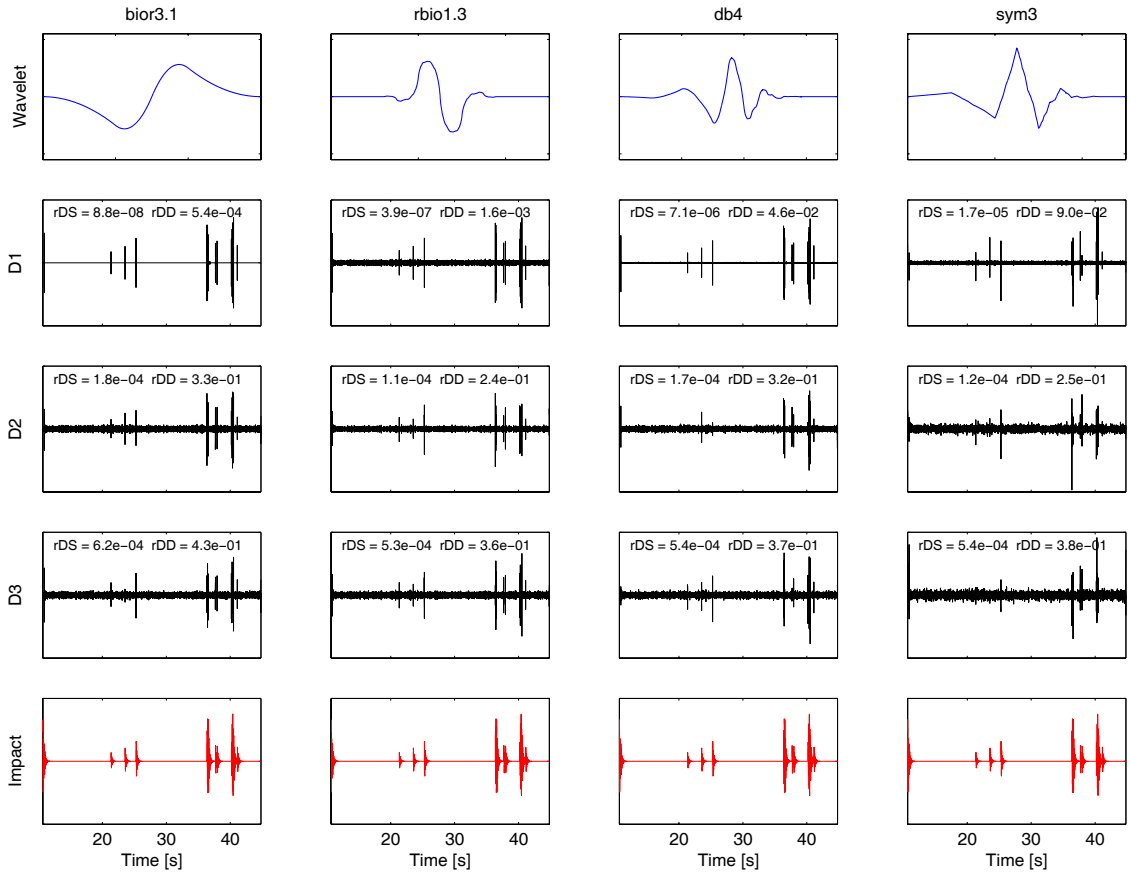

Fig. 13. *Four "best" wavelets to detect impactings in the simulated signals*

conditions to detect impactings.

Concluding the current section we summarise as follows:

- Wavelet analysis is very efficient in recovering weak signals out of noisy input provided we know the structure of the signal;
- One-level wavelet analysis is sufficient to effectively detect impactings;
- Easy-to-implement algorithms based on finding spikes in the first-level details may uncover every single impacting even of a small amplitude.

3.5 Direct application of wavelet analysis to real data

Despite our original expectations, wavelet filtered real signals do not show clear peaks similar to that of the simulated problem (cf. Fig. 13) as seen in Fig. 14.

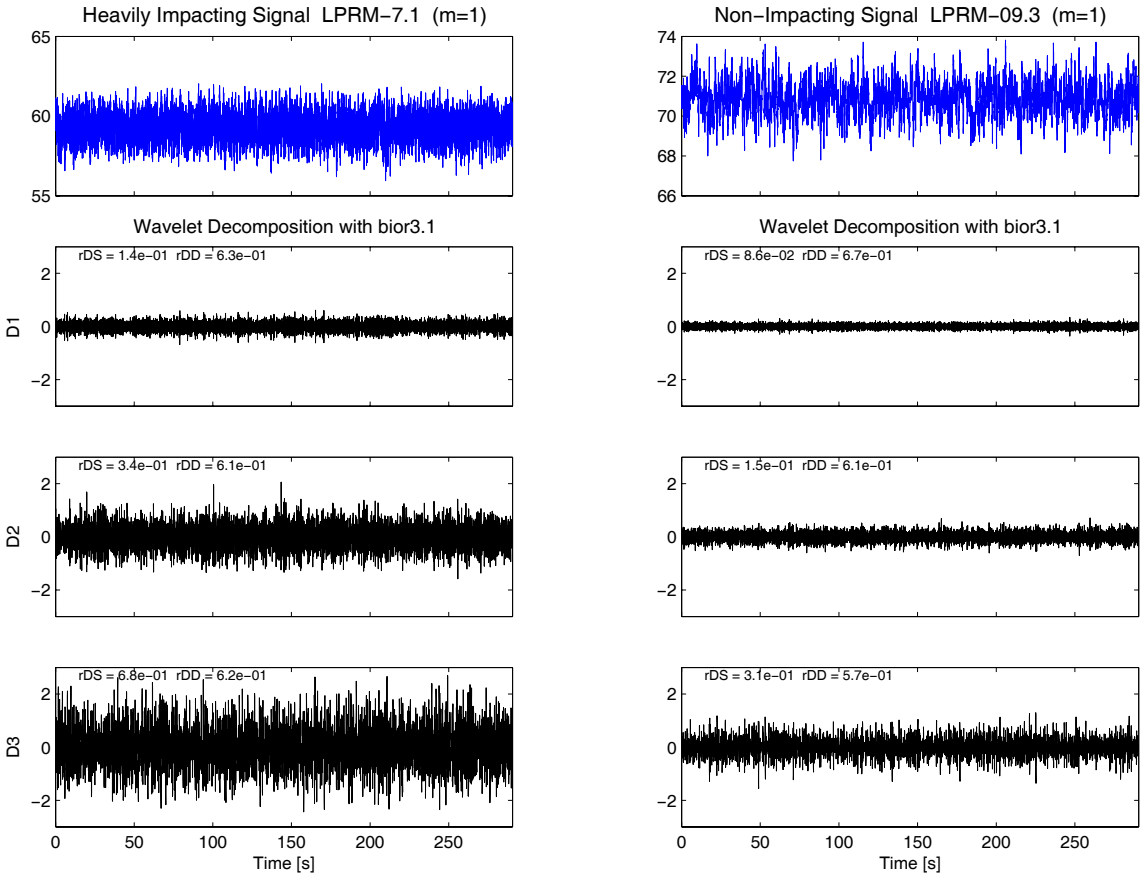

Fig. 14. *Impacting versus Non-Impacting signals in measurement 1*

One reason for this may be the fact that our knowledge about the character of the signals investigated is much less definite than in the case of the simulated signals. The presence of the short transient is a hypothesis that cannot be confirmed experimentally. Further, the eigenfrequency of these hypothetical vibrations is not known either. Altogether, one may conclude that direct application of wavelet analysis to the real data gives somewhat unsatisfactory results, which calls for further analysis and more involved methods. This is the subject of the next Sections.

3.6 Wavelets and frequency

To improve the situation we first turn to frequency considerations. Indeed, we should closely investigate a frequency region near the fuel box eigenfrequency f_0 about which we make an assumption:

$$7Hz \le f_0 \le 20Hz \tag{40}$$

The first step is to establish a relationship between scale (level) and frequency. As for the scale, say a, and level, j, they are related to each other as

$$a = 2^j \tag{41}$$

when we deal with the discrete wavelets.

The desired relationship can be given only in a broad sense, and it is better to speak about the pseudo-frequency corresponding to a scale. If we accept the idea of associating a certain frequency F_c (centre frequency) to the wavelet function, then, when the wavelet is dilated by a factor a, this centre frequency becomes F_c/a. Finally, if the underlying sampling period is Δ, it is natural to associate to the scale a the frequency

$$F_a = \frac{F_c}{a \cdot \Delta} \tag{42}$$

Now the problem reduces to the definition and calculation of the centre frequency. Here the basic idea is to associate with a given wavelet a purely periodic signal of frequency F_c. The frequency maximizing the modulus of the *FFT* (fast Fourier transform) of the wavelet is defined as the centre frequency F_c. Fig. 15 displays some examples of wavelet functions and corresponding purely periodic approximation.

The MATLAB function `centfrq` calculates the centre frequency.

3.7 Further wavelet analysis of the real data

Now, when we are in a position to calculate the frequency corresponding to a scale, let us have a look at the situation at different levels. First we remove the noisy component of a signal S by applying the MATLAB function `wden`. We denote the denoised signal as *Den(S)*. Fig. 16 shows results of the denoising procedure as applied to two extreme cases: heavily impacting and non-impacting signals. The first row of the figure displays the denoised signals when we use a wavelet decomposition (in this case with *bior3.1*) up to level 6 that corresponds to a frequency of about 33 Hz. This level can hardly be useful because the Nyquist frequency is equal to 25 Hz in our case. Level 7 and especially levels 8 (Fa = 8 Hz) and 9 (Fa = 4Hz) give a clear indication that the denoised signal is a smooth function occasionally disturbed by small but sharp and scarce peaks for the non-impacting case (right column). Such a disturbance becomes much more frequent when we turn to a heavily impacting signal (left column).

This gives a motivation to investigate the behaviour of these small peaks. To do so we will need a smoothed signal, which is readily given by the approximation A of a wavelet decomposition. Fig. 17 shows the variation V = *Den(S)*- A of a signal S for the same extreme cases. By calculating the variation V we clean a signal S from all non-stationary

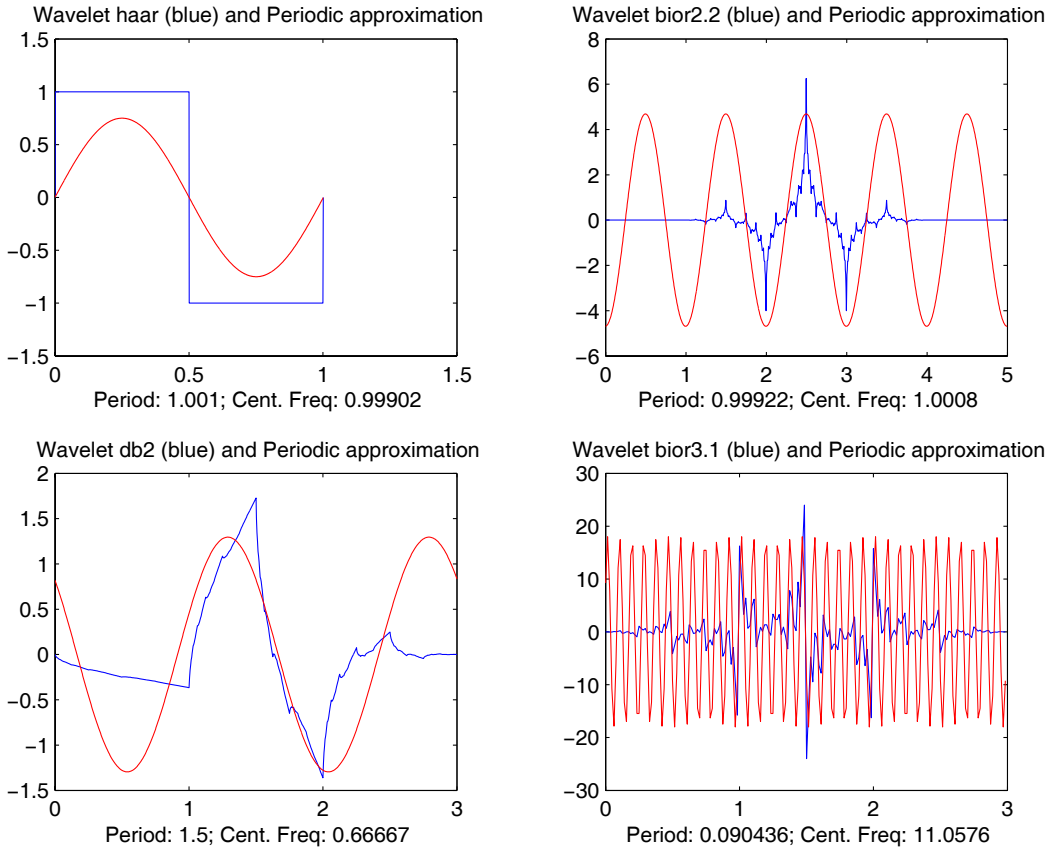

Fig. 15. *Wavelet functions and corresponding centre frequency based approximations*

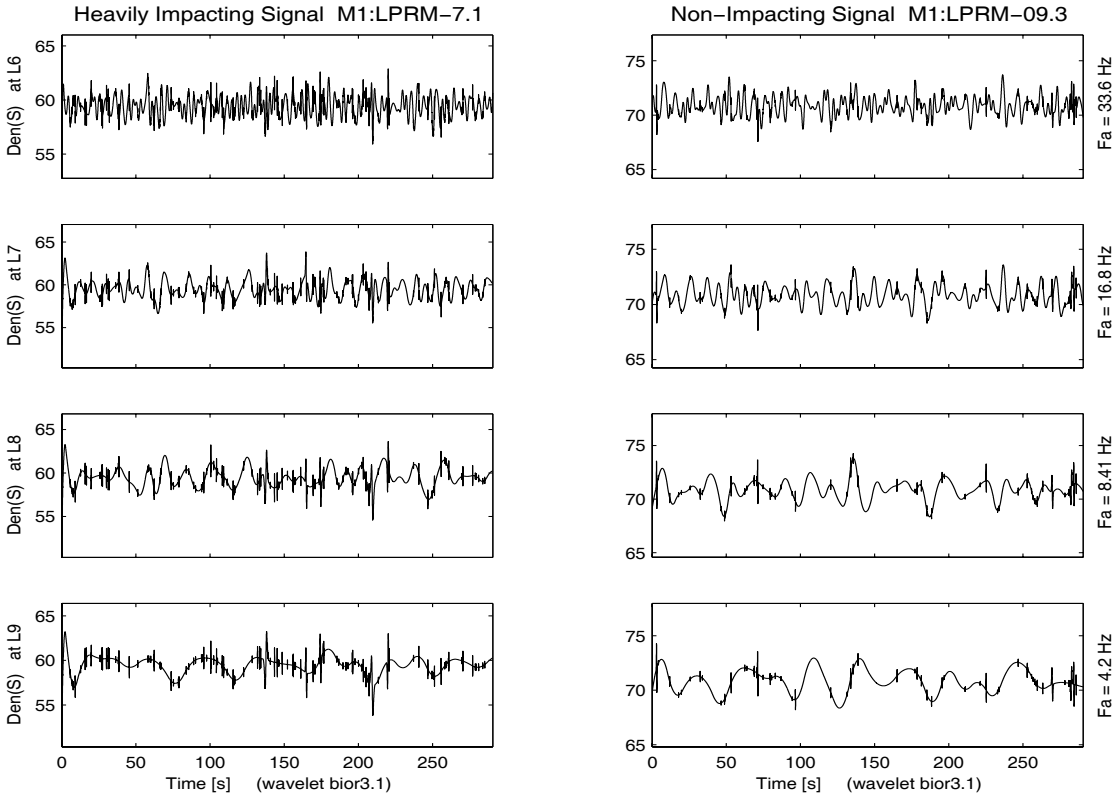

Fig. 16. *Denoised signals, Den(S), for heavily impacting and non-impacting cases as obtained by the wavelet bior3.1 at different levels*

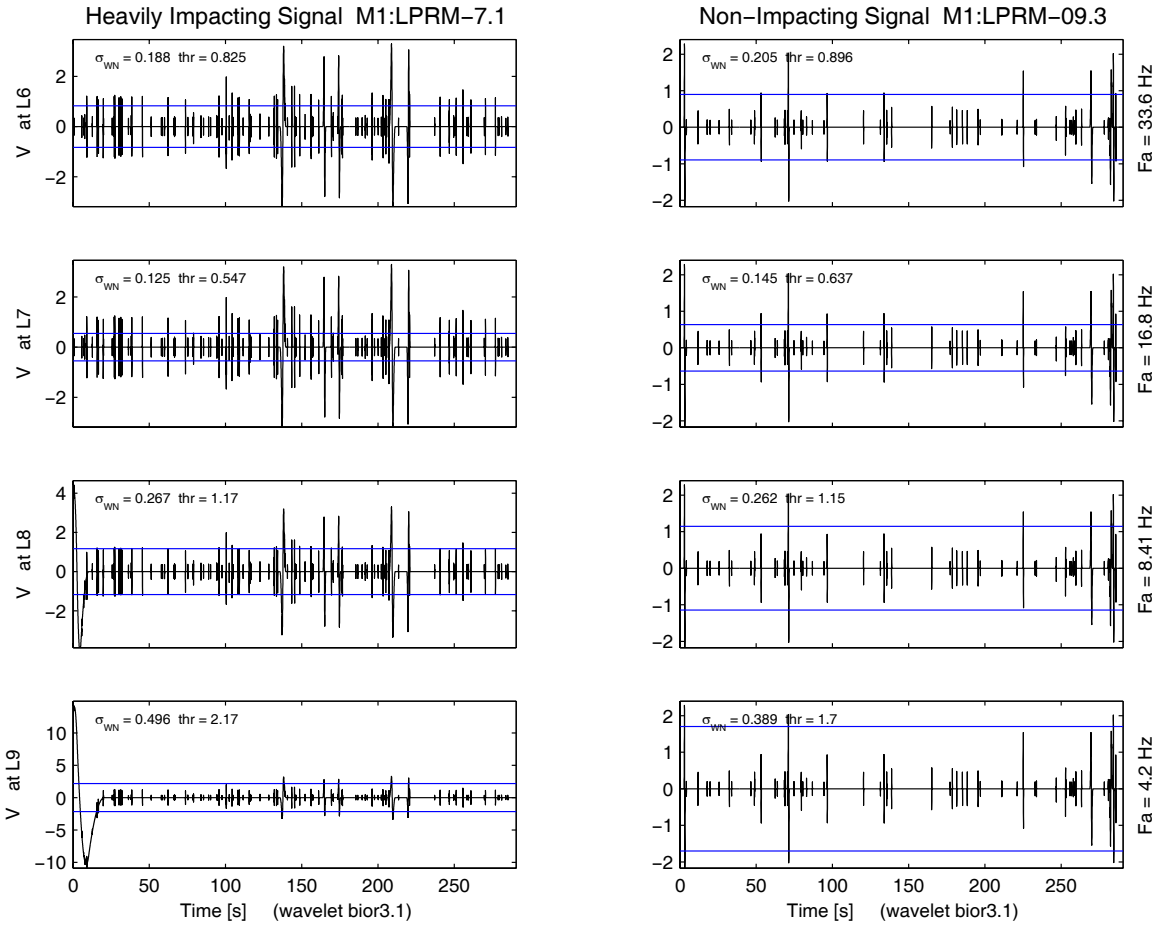

Fig. 17. *Signal variations, V = Den(S) - A, for heavily impacting and non-impacting cases as obtained by the wavelet bior3.1 at different levels*

noise. But some of the peaks due to the global stationary noise are still present in *V*. To eliminate them we need to establish a threshold. At least two such thresholds are proposed in [24] for the case when a signal is contaminated with a Gaussian white noise. In our studies we have used the simplest one assuming, as usual, that the noise is normally distributed:

$$thr \;=\; \sigma_{WN}\sqrt{2\log N} \tag{43}$$

Here σ_{WN} is the variance of the Gaussian white noise and N is the length of the signal (number of samples).

To use the threshold defined in (43) we need an estimate of the white noise variance. According to our theoretical model, the signal consists of a stationary and a non-stationary component and a global noise. The stationary component corresponds to a detector string vibration and occurs at approximately 2-4 Hz, the non-stationary component is due to a fuel box vibrations and occurs in the frequency region 7 to 20 Hz. Denoting a high pass filter with a cut-off frequency f as HP_f, the stationary component as S_S, and transient component as S_T, we have

$$S_f \equiv HP_f(S) \;=\; HP_f(S_S + S_T + WN) \approx HP_f(WN) \Rightarrow \sigma_{WN} \approx std(S_f) \tag{44}$$

if we choose the cut-off frequency f to be greater than the eigenfrequency of the fuel box f_0. A reasonable guess regarding the cut-off frequency f (and probably f_0) may be made by studying how $std(S_f)$ depends on the frequency f. Two typical examples corresponding to extreme cases are shown in Fig. 18. As one can see, normally there is a linear region between 7 to 20 Hz, where the high-pass filter leaves out only the white noise component.

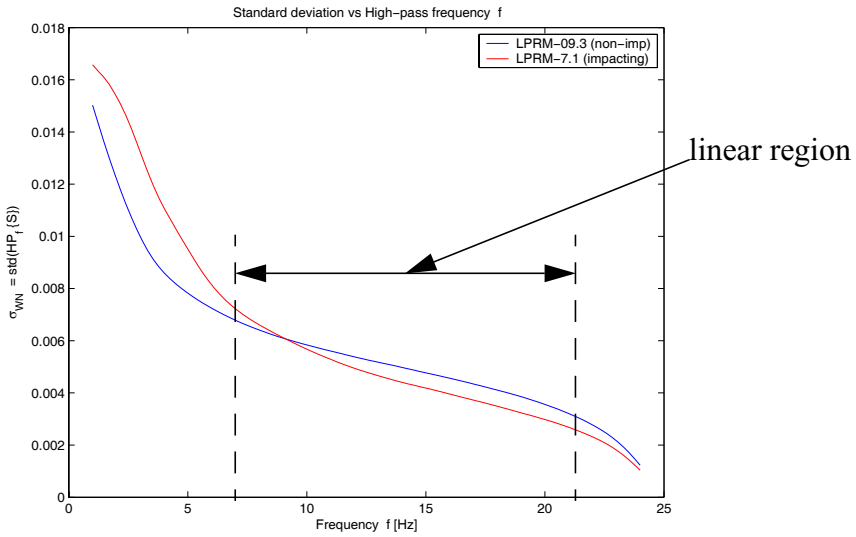

Fig. 18. *Standard deviation vs High-pass frequency*

3.8 Wavelet-based algorithm

All this gives us grounds to formulate the following algorithm to detect impacting:

- choose (arbitrarily) a wavelet function ψ;
- set a frequency F_0 = 12 Hz (this may depend on the specific case under investigation);
- find an optimal level j that minimizes the functional $\min_j |F_c(j, \psi) - F_0|$ where $F_c(j,\psi)$ is the centre frequency of the wavelet ψ at level j;
- calculate the frequency F_a corresponding to the optimal scale $a = 2^j$, $F_a = \dfrac{F_c}{a \cdot \Delta}$;
- set the cut-off frequency $f = F_a$ for the high-pass filter HP_f;
- evaluate the standard deviation of the white noise $\sigma_{WN} = std[HP_f(S)]$;
- calculate the threshold $thr = \sigma_{WN}\sqrt{2\log N}$;
- perform a multi-level wavelet decomposition at the level j;
- denoise a signal S using the MATLAB function `wden`;
- calculate the variation $V = Den(S) - A$;
- remove the peaks below the threshold thr: $V_i = \begin{cases} 0 & if \quad |V_i| < thr \\ V_i & otherwise \end{cases}$
- calculate an impacting rate as a number of non-zero components in V per unit time.

It should be noted here that the impacting rate can be calculated in two different ways: first, to treat a group of non-zero consecutive components V_i as only one peak, in this case we denote the impacting rate as *ir*; second, to make no difference between non-zero components i.e. to count all of them, which is denoted as *IR*.

3.9 Performance of the algorithm

To test the algorithm against real data we have chosen measurement 7 as the most representative example. In order to quantify the performance we calculate a correlation coefficient between the real data and the results produced by the algorithm. The evaluated damage, determined by an expert during a visual inspection and reported in [25] and [26] is collected in a vector d_i where i runs from one to the number of LPRM signals (=24). The correlation between two signals X and Y is defined as

$$\rho(X, Y) = \frac{Cov(X, Y)}{\sigma_X \sigma_Y}; \qquad Cov(X, Y) = E\{(X - \mu_X) \cdot (Y - \mu_Y)\} \tag{45}$$

The algorithm calculates a vector *ir* or *IR* of impacting rates evaluated for each individual LPMR signal. In the next pictures we present either the correlation $\rho(d, ir)$, denoted simply as *ir*, or $\rho(d, IR)$ denoted as *IR*. A representative selection of wavelets available in MATLAB has been made. It includes 5 families: Daubechies *db1* to *db16*, Biorthogonal *bior1.1* to *bior6.8*, Reverse Biorthogonal *rbio1.1* to *rbio6.8*, Symlets *sym1* to *sym16*, and finally Coiflets *coif1* to *coif5* plus Discrete Mayer *dmey.* The overall performance is presented in Fig. 19 and Fig. 20.

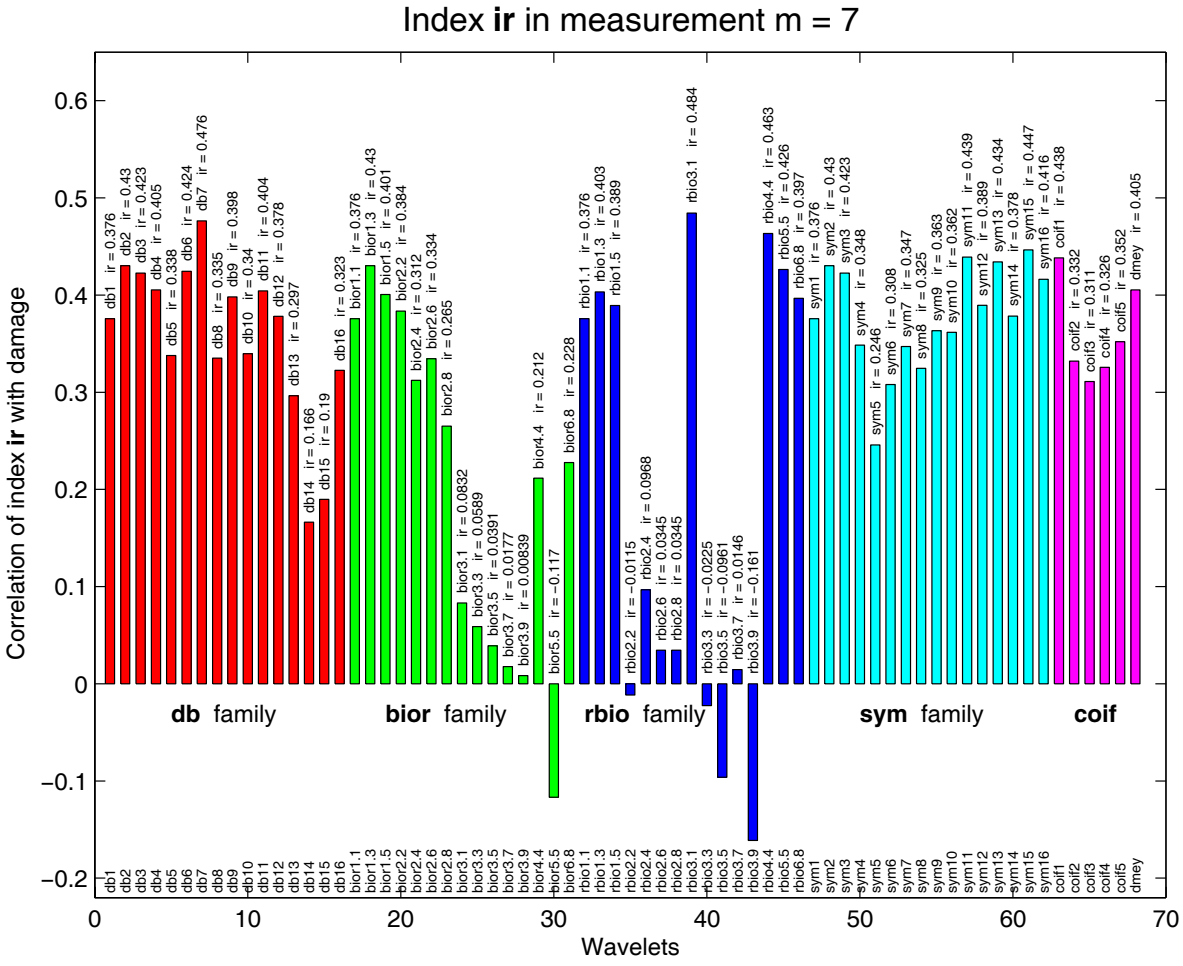

Fig. 19. *Impacting rate index ir shown by various wavelets*

On comparing Fig. 19 and Fig. 20 we may conclude that the *IR* indicator (all individual spikes counted separately) is better correlated with the damage than its counterpart *ir*.

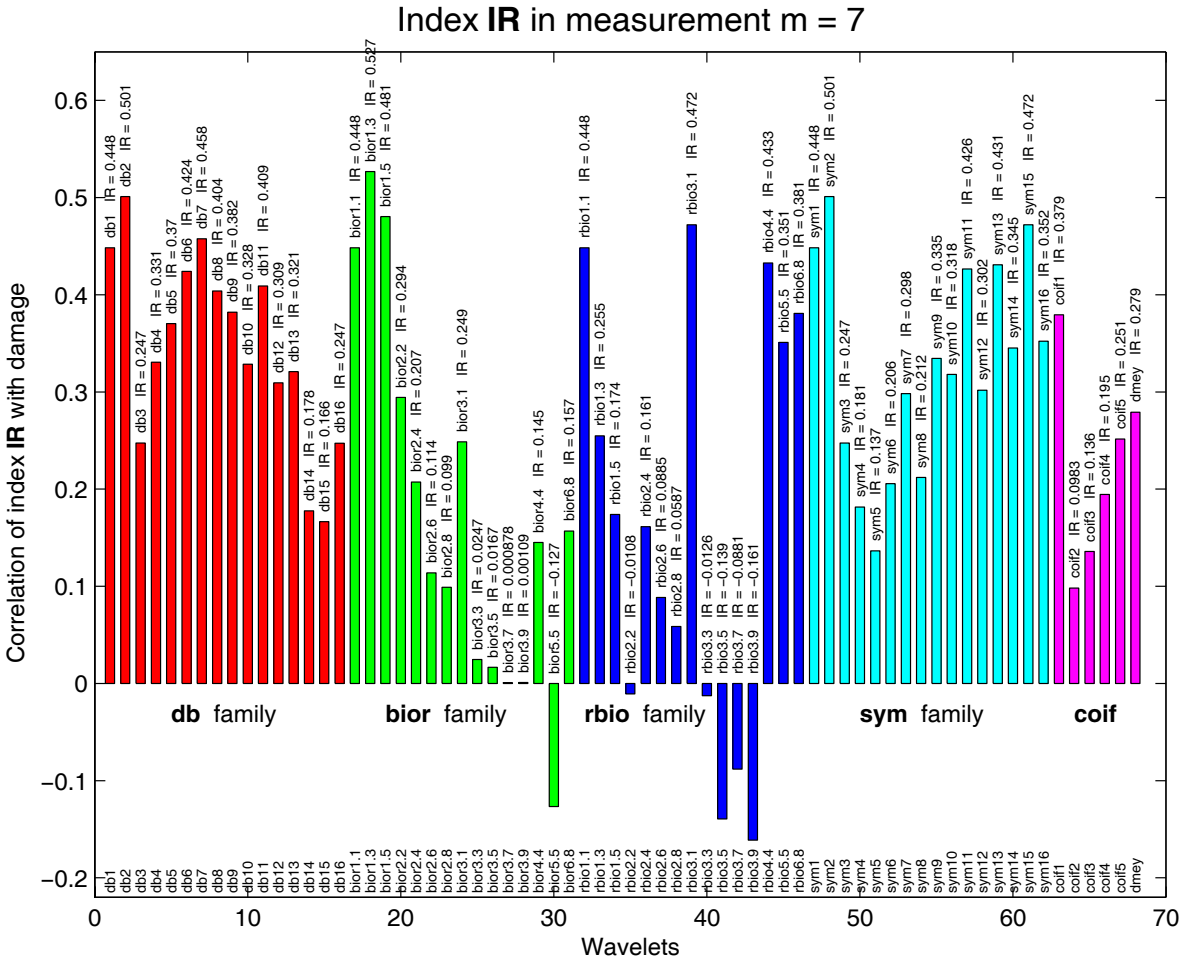

Fig. 20. *Impacting rate index IR shown by various wavelets*

A sorted list of correlations is presented in Fig. 21 which shows that the best wavelets are different from those expected from the simulated signals. They are *rbio1.3, sym2, db2, and bior1.3*. The best wavelet function, *rbio1.3* yields a correlation of 0.53, which considerably improves the performance of the Haar wavelet, 0.38 as reported in [7], and exceeds the best non-wavelet indicator, namely the power peak at the second eigenfrequency, pp2, that showed a correlation of 0.43 [7].

In Fig. 22 we display an example of how the best four wavelets process real signals shown in black and which are taken from Measurement 1. It should be noted here that the plotting program automatically uses a randomly generated vector with the normal distribution *N(0,1)* as an input signal when a corresponding real signal is absent or corrupt. In Fig. 22 rows 3 and 6 correspond to such vectors. It gives us an opportunity to evaluate the performance of the algorithm against purely random and thus non-impacting signals.

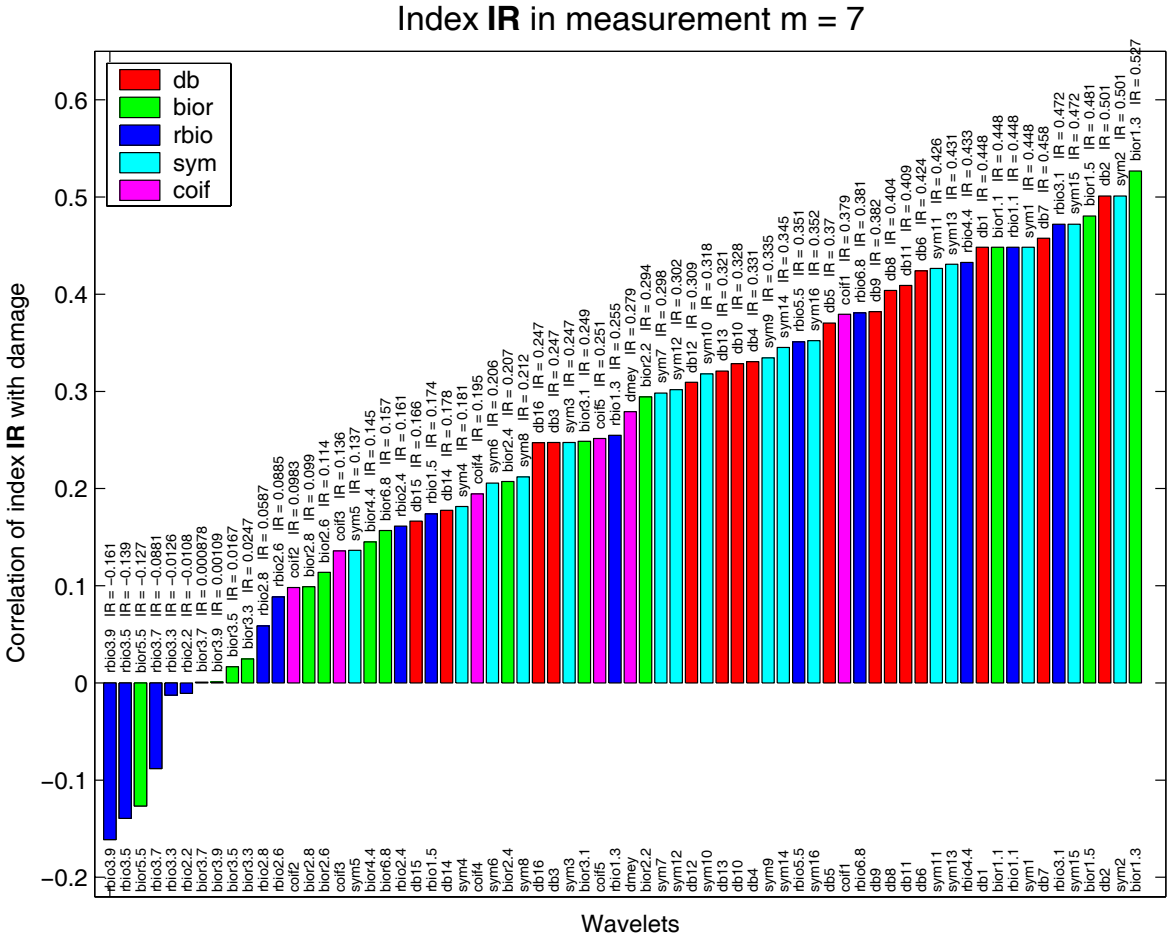

Fig. 21. *Wavelets sorted w.r.t. correlation*

3.10 Conclusions

Access to the data taken in Oskarshamn-2 has given an outstanding opportunity to test and develop algorithms for detecting and quantifying detector tube impacting. In this Stage, first a thorough check of the wavelet functions available in MATLAB has been performed by using simulated signals. The analysis showed that the wavelet technique is a very powerful general method to extract weak signals deeply hidden in a noisy background provided that we know the structure of a signal. Because of this, a physical model of impacting is first presented in the report. Contrary to our original expectations, a direct (and somewhat simplified) application of wavelet methodology produced very poor results. It turned out that a more involved wavelet analysis is needed to obtain satisfactory results. As a consequence, a general algorithm to detect impactings has been developed. The algorithm has no phenomenological (arbitrary) factors to tune its performance. On contrary, it has only one physically grounded parameter F_0 and few parameters that determine the wavelet denoising procedure. In addition, we note here that the algorithm automatically selects an optimal level of the wavelet decomposition, taking a wavelet function as an input parameter. All this provided an opportunity to investigate a broad variety of wavelet functions available in MATLAB. The result of this investigations summarized in a performance-sorted list of wavelets, where the best wavelet function shows a correlation of 0.53. This is considerably better than the efficiency of the Haar wavelet in the previous work (0.38), and exceeds the

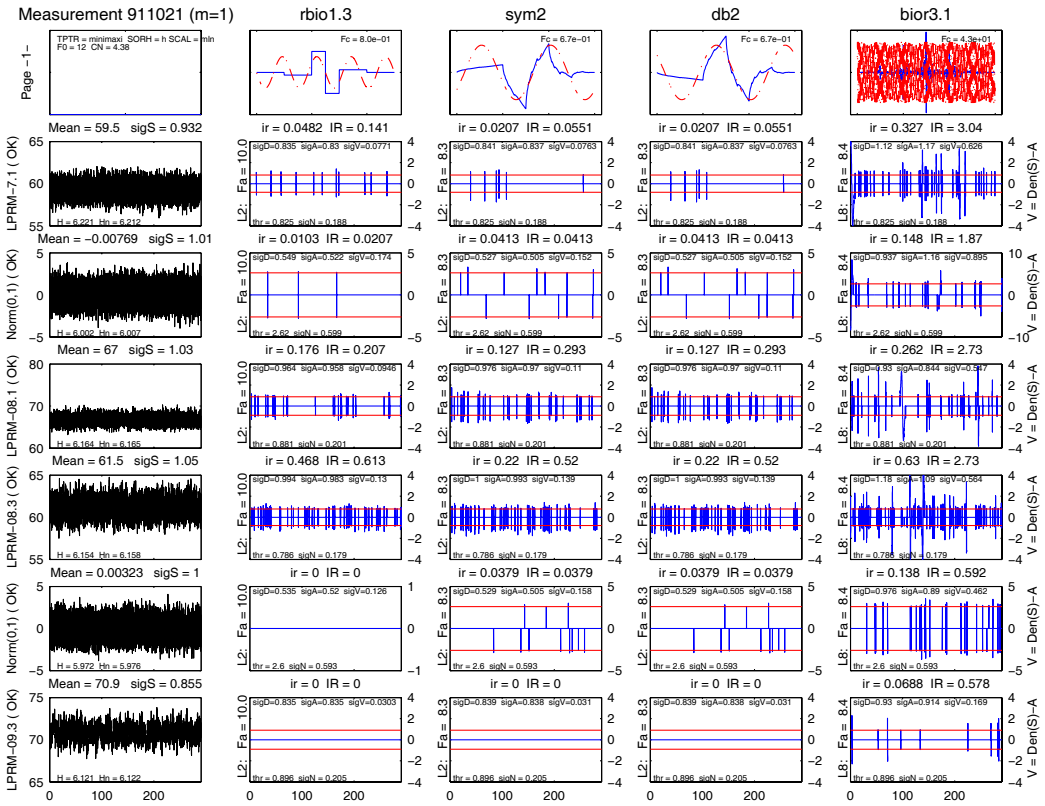

Fig. 22. *The best four wavelets*

best non-wavelet indicator, pp2, whose performance of 0.43 was reported in the previous report [7].

Plans for the continuation

In stage 9 we plan to include the following parts in the current R&D program:

- Final evaluation of the wavelet technique for detector impacting
- Development of the theory of systems with a non-stationary boundary
- Theory of the dynamics of source-driven subcritical systems
- Preparations for pilot measurements with a prototype Cf-252 detector
- Dynamic space-resolved single-phase flow measurements with laser and paint mixed in the water.

Acknowledgement

This project was supported by the Swedish Nuclear Power Inspectorate, contract No. 14.5-010892-01161. Ewa Kurcyusz-Ohlofsson, from Vattenfall Fuel AB, is acknowledged for the delivery of the SIMULATE-3 output data.

REFERENCES

[1] Pázsit I., Garis N. S. "Forskningsprogram angående härddiagnostik med neutronbrusmetoder." *Etapp 1. Slutrapport, SKI Rapport* 95:14 (1995)

[2] Pázsit I., Garis N. S., Thomson O. "Forskningsprogram angående härddiagnostik med neutronbrusmetoder." *Etapp 2. Slutrapport, SKI Rapport* 96:50 (1996)

[3] Pázsit I., Garis N. S., Karlsson J., Rácz A. "Forskningsprogram angående härddiagnostik med neutronbrusmetoder." *Etapp 3. Slutrapport, SKI Rapport* 97:31 (1997)

[4] Pázsit I., Karlsson J. K-H., "Research and Development Program in Reactor Diagnostics and Monitoring with Neutron Noise Methods." *Stage 4. Final Report, SKI Report* 98:25 (1998)

[5] Pázsit I., Karlsson J. K-H., Lindén P., Arjanov V. "Research and Development Program in Reactor Diagnostics and Monitoring with Neutron Noise Methods." *Stage 5. Final Report, SKI Report* 99:33 (1999)

[6] Pázsit I., Demazière C., Avdic S., Dahl B. "Research and Development Program in Reactor Diagnostics and Monitoring with Neutron Noise Methods." *Stage 6. Final Report, SKI Report* 00:28 (2000)

[7] Pázsit I., Demazière C., Arzhanov V., and Garis N. S. "Research and Development Program in Reactor Diagnostics and Monitoring with Neutron Noise Methods." *Stage 7. Final Report, SKI Report* 01:27 (2001)

[8] Umbarger J. A., DiGiovine A. S., *SIMULATE-3, Advanced Three-Dimensional Two-Group Reactor Analysis Code, User's Manual*, Studsvik Report, Studsvik of America (1992)

[9] Nakamura S., *Computational Methods in Engineering and Science With Applications to Fluid Dynamics and Nuclear Systems*, Wiley Interscience, New York (1977)

[10] Bell G. I., Glasstone S., *Nuclear Reactor Theory*, Van Nostrand Reinhold Company, New York (1970)

[11] Demazière C. "Theoretical and Numerical Evaluation of the MTC Noise Estimate in

2-D 2-group Heterogeneous Systems." *SKI Report* 02:37 (2002)

[12] Engström S., Forsmark internal report FT-Rapport 96/326 (in Swedish) (1996)

[13] Pázsit I. "Determination of reactor stability in case of dual oscillations," *Annals of Nuclear Energy*, **22**, pp. 377-387 (1995)

[14] D'Auria F. et al. "State of the Art Report on Boiling Water Reactor Stability – Appendix B: Methods for Evaluating Decay Ratio," NEA report NEA/CSNI/R(96)21, pp. 333-341 (1997)

[15] Oguma R. "Application of Noise Analysis for the Study of Core Local Instability at Forsmark 1," *SKI Rapport* 97:42 (1997)

[16] Karlsson J. K. -H., and Pázsit I. "Localisation of a channel instability in the Forsmark-1 boiling water reactor," *Annals of Nuclear Energy*, **26**, pp. 1183-1204 (1999)

[17] Demazière C. and Pázsit I. "2-D 2-group neutron noise simulator and its application to anomaly localization," *Proceedings of M&C2001*, Salt Lake City, Utah, USA, September 9-13, 2001 (2001)

[18] Lansåker P., Forsmark internal report FT-Rapport 97/485 (in Swedish) (1997)

[19] Analytis G. Th., Hennig D., and Karlsson J. K. -H., "The physical mechanism of core-wide and local instabilities at the Forsmark-1 BWR," *Nuclear Engineering and Design*, **205**, pp. 91-105 (2001)

[20] Hotta A., "Numerical study on observed decay ratio of coupled neutronic-thermal hydraulic instability in Ringhals Unit 1 under random noise excitation," *Journal of Nuclear Science and Technology*, **39**, pp. 138-149 (2002)

[21] Pázsit I., Glöckler O. "BWR Instrument Tube Vibrations: Interpretation of Measurements and Simulation", *Ann. nucl. Energy* **21**, 759 - 786 (1994)

[22] Thomson O., Garis N. S. and Pázsit I. "Quantitative analysis of detector string impacting", *Nuclear Technology* **120**, 71 (1997)

[23] Rácz A. and Pázsit I. "Detection of detector string impacting with wavelet techniques", *Ann. nucl. Energy* **25**, 387-400 (1998)

[24] Mallat S., *A Wavelet Tour of Signal Processing*, Academic Press, USA (1999)

[25] Karlsson J. K.-H., Bergdahl B.-G., Oguma R. "The guide tube vibrations at Oskarshamn-2 1991-1994", *GSE Power Systems AB*, GSE-01-006 (2001)

[26] Bergdahl B-G. and Oguma R. "Investigation of In-Core Instrument Guide Tube Vibrations at Oskarshamn BWR Unit 2 Based on Noise Analysis", *SKI Rapport* 96:37 (1996)